



# Climate change impact to Mackenzie river Basin projected by a regional climate model

Chun-Chao Kuo<sup>1,2</sup> · Thian Yew Gan<sup>1</sup> · Jingwen Wang<sup>1</sup>

Received: 16 February 2019 / Accepted: 20 February 2020 / Published online: 11 March 2020  
© Springer-Verlag GmbH Germany, part of Springer Nature 2020

## Abstract

A regional climate model, WRF (Weather Research and Forecasting model), was set-up and fine-tuned to simulate the possible impacts of climate change to the Mackenzie River Basin (MRB) of Canada from May to October. The baseline (1979–2005) regional climate of the MRB simulated by WRF agrees well with gridded observed climate data, ANUSPLIN of Environment Canada. Next, WRF projected the regional climate change of MRB for 2041–2100 by dynamic downscaling RCP4.5 and RCP8.5 climate scenarios of three global climate models (GCMs), ACCESS1–3, CCSM4, and CanESM2. Based on RCP4.5 and RCP8.5 climate scenarios downscaled by WRF, air temperature of MRB is projected to increase by 2.5–3.8 °C and 4.5–6.9 °C in the 2050 s and 2080 s, respectively. In general, the air temperature of MRB is projected to increase marginally higher in colder regions of higher latitude and elevation. In contrast, the seasonal precipitation of MRB is only projected to increase marginally in the 2080 s under the RCP4.5 and RCP8.5 scenarios, respectively. The projected extreme precipitation indices show that future precipitation events would become more intensive and of longer durations. Under both RCP4.5 and RCP8.5 climate scenarios, the annual counts of days with total precipitation exceeding 10 mm of MRB (R10mm) are projected to increase by 18% in 2041–2100; the maximum 5-day precipitation (Rx5day) could increase by 9.4%. More studies should be conducted to gain a better understanding of the potential impacts of global warming to MRB and possible adaptive measures to mitigate these impacts.

**Keywords** Mackenzie River Basin · Climate change impact · Precipitation · Temperature · Regional climate model WRF · RCP 4.5 · 8.5 climate scenarios

## 1 Introduction

Possible changes to the water resources of a watershed under climate change impact would affect its future management and planning. Assuming climate remains stationary, historical hydrologic observations of a watershed should remain more or less unchanged in the future. However, historical measurements of hydrological variables of river basins across the world in terms of trends and variabilities have shown various degrees of changes (e.g. Brabets and

Walvoord 2009; Mekis and Vincent 2011; Vincent et al. 2012; Dibike et al. 2012; Fu et al. 2015; Kukal and Irmak 2016), including the Mackenzie River Basin (MRB) of Canada (Aziz and Burn 2006; Burn 2008; Bawden et al. 2014; Yang et al. 2015), Alberta (Jiang et al. 2015), and other parts of Canada (Tan and Gan 2015). These hydrologic changes will likely affect the availability of water resources, ecology, biodiversity, and water quality of river basins, which will incur new challenges to managing the water resources of these river basins.

The analysis of climatic trends from past observations provides some insights to climatic changes in recent decades. Projected changes to atmospheric conditions due to the radiative forcing of rising concentrations of greenhouse gases (GHG) such as CO<sub>2</sub> and methane have been mostly based on Representative Concentrated Pathways (RCPs) climate scenarios simulated by various Global Climate Models (GCMs) of the Coupled Model Intercomparison Project Phase 5 (CMIP5) of the Intergovernmental Panel on Climate

✉ Thian Yew Gan  
tgan@ualberta.ca

<sup>1</sup> Department of Civil and Environmental Engineering, Innovation Centre for Engineering, University of Alberta, 7-230 Donadeo, 9211-116 Street NW, Edmonton, AB T6G 1H9, Canada

<sup>2</sup> River Forecast Centre, Government of British Columbia, Nanaimo, Canada

Change (IPCC) in its fifth assessment report (AR5) (IPCC 2013). Such RCP scenarios simulated by GCMs to account for the projected rising concentrations of GHG have been widely used to assess the hydrologic impacts of climate change (e.g. Arora et al. 2011; Deng et al. 2013; CSIRO and Bureau of Meteorology 2015; Pattnayak et al. 2017).

Because of the coarse resolutions of GCMs, for regional impact studies, RCP climate scenarios are mostly down-scaled, either by statistical methods (Pacific Climate Impacts Consortium 2014; Shashikanth et al. 2014; Gutmann et al. 2014; Mehrotra and Sharma 2010), or by dynamic models (Giorgi et al. 2009; Dibike et al. 2012; Ishida et al. 2017; Ozturk et al. 2017) to project regional climate at spatial and temporal resolutions adequate for regional studies. Since the statistical downscaling approach is computationally modest, it is readily applicable to areas of interest, based on climate change projections of many GCMs. However, the skills of statistical downscaling approaches depend on the availability of representative historical observations to develop physically meaningful empirical relationships for climate variables, and the assumption is that the statistical relationship between the predictors and predictands will remain unchanged in the projected periods. Therefore, the density of observed networks in relation to the resolutions of GCMs are critical to statistically downscale climate variables of GCMs to dependable, regional rainfall and hydrological variables (Shashikanth et al. 2014). On the other hand, the dynamical downscaling approach uses an RCM (Regional Climate Model) driven by initial and lateral boundary conditions based on the simulations of GCMs. This approach accounts for physical mechanisms within the simulation domains instead of an empirical, “black box” relationship developed between climate variables of fine and coarse resolutions. Even though dynamic downscaling is more physically vigorous, it is computationally expensive, so a regional climate change study by this approach is often achievable with only a limited number of climate change projections of GCMs.

Regional projections of precipitation and air temperature are needed to assess different types of climate change impacts, such as hydrologic (Jha et al. 2004; Herrera-Pantano and Hiscock 2015), environmental/ecologic (Whitehead et al. 2013; Trang et al. 2017), and economic impacts (Whitehead et al. 2013; Gaudard et al. 2014; de Queiroz et al. 2016). For example, hydrological models driven by projected precipitation and air temperature are used to simulate water cycle changes, especially streamflow, to evaluate the hydrologic impacts of climate change (Al Aamery et al. 2016; Eum et al. 2017; Tan et al. 2017; Kuo et al. 2017), which could be further applied to assess the impacts of climate change on water quality (e.g. Wilson and Weng 2011; Xia et al. 2015), ferry operations (Zheng and Kim 2017; Du

et al. 2017), river ice break-up (Lesack et al. 2014; Beltos 2008), flood, and drought (Zhang et al. 2019).

The Coordinated Regional Climate Downscaling Experiment (CORDEX; Giorgi et al. 2009) is a program initiated by the World Climate Research Program. Different regional climates simulated by selected GCMs are downscaled by selected RCMs to provide global coverage for projected air temperature and precipitation at regional scales at about 50-km resolution. There have been limited studies conducted on basin-scale analyses of air temperature and precipitation projected for northern river basins.

Given climate change projections of fine spatial resolutions are necessary to investigate regional climate change impacts, the objectives of this study are to investigate: (a) the bias of modeling the regional climate of the MRB using the WRF (Weather Research and Forecasting Model) (Skamarock et al. 2008) driven by RCP climate scenarios of three different GCMs (CanESM2, CCSM4, and ACCESS1-3), (b) the bias of WRF simulations in relation to terrain features of MRB, (c) the effectiveness of the delta change bias correction method on the bias correction of seasonal air temperature, precipitation and six extreme precipitation indices of MRB, and (d) projected changes of seasonal precipitation, air temperature, and six extreme precipitation indices in 2041–2100 for MRB under RCP4.5 and RCP8.5 climate scenarios. The definitions of the six extreme precipitation indices are described in the followings. R10mm is the count of days with total precipitation exceeding 10 mm (Karl et al. 1999; Peterson et al. 2001) while CDD (CWD) is the maximum number of consecutive days with daily precipitation less (equal and more) than 1 mm. Rx1day (Rx5day) is the maximum 1-day (5 consecutive days) precipitation, and SDII is the simple precipitation intensity index (mm/day) that represents the average precipitation intensity of wet days, or the sum of the daily precipitation of wet days (daily precipitation  $\geq 1$  mm) divided by the number of wet days. SDII represents the average precipitation intensity for the wet days.

## 2 Study domain and datasets

This study focuses on the largest river basin of Canada, the Mackenzie river basin (MRB) which occupies a geographic region extending from central Alberta to the Arctic Ocean, with an area of about  $1.8 \times 10^6$  km $^2$  (shown in the central thick lines of Fig. 1). MRB has three major lakes and many small lakes and wetlands (fens and bogs), and a wide range of elevations between several meters to over 3000 meters at Canadian Rocky Mountains. Its mean annual air temperature

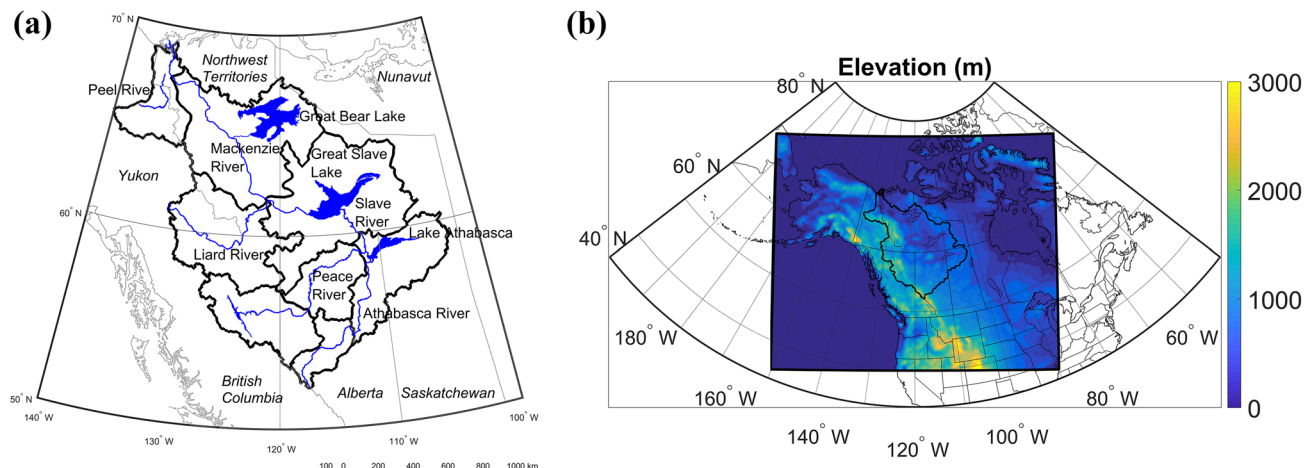


**Fig. 1** **a** The tributaries and lakes in Mackenzie River Basin, provinces and territories (in Italic) of northwestern Canada; **b** The domain set-up for the Mackenzie River Basin of Canada. Climate scenarios of CanESM2, CCSM4, and ACCESS1-3 are downscaled by WRF for this domain

ranges from  $-10$  to  $4$   $^{\circ}\text{C}$ , and its precipitation is highly variable spatially, ranging from less than  $200$  mm/year along the arctic coast to more than  $1000$  mm/year in the southwest of MRB (Woo and Thorne 2003; Woo et al. 2014). The mean annual precipitation is about  $410$  mm.

The initial and lateral boundary climate conditions of three Global Climate Models (GCMs), CanESM2, CCSM4, and ACCESS1-3 (Table 1) that represent wet, normal, and dry climate projections within the study domain, are selected to drive WRF in simulating the baseline and the future climate of MRB. The ANUSPLIN data of Environment and Climate Change Canada (McKenney et al. 2006; Hutchinson et al. 2009) is used as the reference to assess the simulated regional climate of MRB using WRF. The ANUSPLIN data uses the thin plate smoothing spline algorithms to prepare the gridded daily maximum and minimum temperature, and precipitation data at  $10$  km by  $10$  km spatial resolution covering Canada.

The mean absolute errors in daily maximum and minimum temperature, and precipitation for Canada are about  $1.18$   $^{\circ}\text{C}$ ,  $1.68$   $^{\circ}\text{C}$ , and  $2.9$  mm, respectively (Hutchinson et al. 2009), while the mean percent absolute errors in total annual precipitation is about  $9\%$ . In general, the errors of

these variables are lower in summer and autumn than in spring and winter. It should be noted that higher biases in air temperature are found in Yukon and British Columbia probably because of relatively few climate stations and typical temperature-elevation gradients related to the effects of cold air around Rocky Mountains (Hutchinson et al. 2009). However, the residual trend of precipitation bias with respect to elevation has been shown to be relatively minimal.

Two future climate scenarios, RCP 4.5 and 8.5 are selected for this study. Given the radiative forcing of RCP4.5 climate scenarios peaks at about  $4.5$   $\text{W}/\text{m}^2$  ( $\sim 540$  ppm  $\text{CO}_2$ ) in 2100, this RCP climate scenario is roughly comparable to the SRES (Special Report Emission Scenario) B1 scenario in terms of projected  $\text{CO}_2$  concentrations and median temperature increase by 2100. The RCP8.5 climate scenarios assume a higher radiative forcing increase, peaking at  $8.5$   $\text{W}/\text{m}^2$  ( $\sim 940$  ppm  $\text{CO}_2$ ) in 2100, which means a higher projected  $\text{CO}_2$  concentrations than those of SRES A2 climate scenarios by 2100 (IPCC 2007, IPCC 2013), e.g., RCP 8.5 is the climate scenario that projects the highest GHG concentration levels compared to other RCP climate scenarios (Riahi et al. 2011).

**Table 1** Selected GCMs from the CMIP5 experiment (IPCC, 2013) used in this study

Model designation	Climate modeling group	Group Acronym	Country
ACCESS1-3	Commonwealth Scientific and Industrial Research Organisation (CSIRO) and Bureau of Meteorology (BOM)	CSIRO-BOM	Australia
CanESM2	Canadian Centre for Climate Modelling and Analysis	CCCMA	Canada
CCSM4	National Centre for Atmospheric Research	NCAR	USA

Projected climate variables under the RCP4.5 and RCP8.5 scenarios are downscaled from the selected models to a 30-km resolution over the MRB using WRF

### 3 Research methodology

#### 3.1 WRF configurations

WRF was set up in one-domain framework covering most of western North America at 30 km x 30 km resolution (Fig. 1) and the model domain is configured with 28 vertical levels with the top level at 100 hPa. Through tests conducted by Kuo and Gan (2018), the Yonsei University planetary boundary layer (PBL) scheme (Hong et al. 2006), the WRF Double-Moment 6-class scheme (Lim and Hong 2010), Kain-Fritsch scheme (Kain 2004), and the Longwave (LW) and Shortwave (SW) radiation schemes Community Atmosphere Model (CAM) (Collins et al. 2004) were found to simulate representative regional climate of MRB. Additional variables and options such as the snow depth, the sea ice fraction, and SST updating were also included (Kuo and Gan 2018). Each year, the climate of MRB for April 28th to November 1st are simulated but the first 3-day simulations are discarded as the spin-up period. A total of 27 years (1979–2005) were selected as the baseline climate to assess the accuracy of WRF downscaling of the simulations of CanESM2, CCSM4, and ACCESS1–3. The regional climate of MRB for the future period (2041–2100) was simulated by WRF driven by the simulations of the three selected GCMs.

#### 3.2 Bias of simulated precipitation and air temperature

The bias of the precipitation and air temperature of MRB simulated by WRF is evaluated using (a) difference between the simulated and the observed (ANUSPLIN data), and (b) difference between the simulated and the observed (ANUSPLIN data) air temperature, and (c) Perskins Skill Score (PSS) (Perkins et al. 2007) of the simulations which is designed to assess the goodness-of-fit between the Probability Density Functions of the simulated and observed data. A PSS of one means a perfect fit.

To compare differences between simulated and observed data, the Triangle-based linear interpolation (Watson and Philip 1984) was used to interpolate precipitation and air temperature simulated by WRF at 30-km grid into the 10-km grid of ANUSPLIN. This method first forms the Delaunay triangulation from each grid of WRF and the interpolation point L(x,y) is estimated by

$$L(x, y) = \sum_{i=1}^3 w_i f(x_i, y_i) \quad (1)$$

where the weight  $w_i$ , the  $i$ th barycentric coordinate of L(x,y) with respect to the triangle (Watson 1992) sums up to one.  $f(x_i, y_i)$  is the air temperature or precipitation simulated by WRF at grid  $(x_i, y_i)$ .

#### 3.3 Delta bias correction method

The Delta bias correction method (Lenderink et al. 2007) uses the differences (deltas) between mean observed and mean simulated variables to adjust the current and future projected values. By bias correction of precipitation at each grid, the corrected precipitation is

$$P_{cor} = P_{sim} \times \Delta P \quad (2)$$

where  $\Delta P$  is the ratio for precipitation,  $\Delta P = (\bar{P}_{obs,base}/\bar{P}_{sim,base})$ ,  $P_{sim}$  is the simulated precipitation,  $P_{cor}$  is the corrected precipitation,  $\bar{P}_{obs,base}$  is the mean observed baseline precipitation, and  $\bar{P}_{sim,base}$  is the mean simulated baseline precipitation.

To bias correct air temperature at each grid, the corrected air temperature is

$$T_{cor} = T_{sim} + \Delta T \quad (3)$$

where for air temperature,  $\Delta T = (\bar{T}_{obs,base} - \bar{T}_{sim,base})$ ,  $T_{sim}$  is the simulated air temperature, and  $T_{cor}$  is the corrected air temperature.  $\bar{T}_{obs,base}$  is the mean observed, and  $\bar{T}_{sim,base}$  is the mean simulated baseline air temperature, respectively.

#### 3.4 Detection power

In order to confirm whether the projected changes are higher than the baseline errors, we define the detection power as follows:

$$\begin{aligned} \text{Detection power} &= |V_{change}| - |V_{bias}|, \\ \text{when } (|V_{change}| - |V_{bias}|) &> 0 \end{aligned} \quad (4)$$

$V_{change}$  = NA (Not Applicable),

$$\text{when } (|V_{change}| - |V_{bias}|) \leq 0 \quad (5)$$

where  $V_{change}$  is the future change of variables (precipitation or air temperature) after the bias correction and  $V_{bias}$  is the baseline bias of variables (precipitation or air temperature).

### 4 Discussions of results

#### 4.1 Simulated precipitation and air temperature of the baseline period (1979–2005)

Figure 2 shows the spatial distributions of the mean annual precipitation differences between observed ANUSPLIN data, and that of three GCMs downscaled by WRF for 1979–2005. On a whole, GCMs' output downscaled by

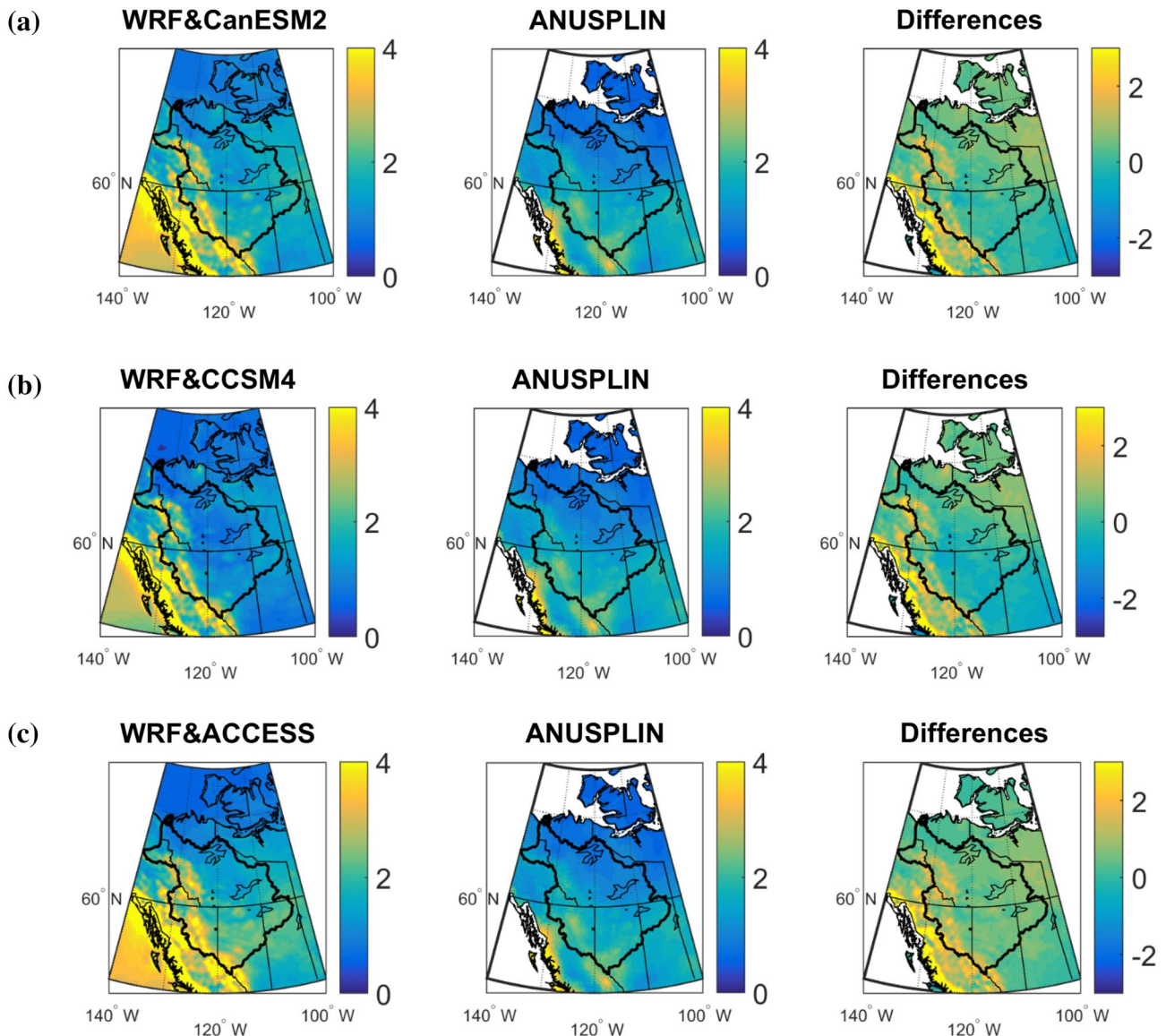


**Fig. 2** The 1979–2005 MJASO (May–October) mean daily precipitation (mm/day) simulated by (left) **a** WRF&CanESM2, **b** WRF&CCSM4, and **c** WRF&ACCESS, ANUSPLIN precipitation data (middle), and the differences (right)

**Table 2** Statistics of the ANUSPLIN data and the baseline precipitation (mm/day) downscaled by WRF at the watershed scale for MJASO

Statistics	ANUSPLIN <sup>a</sup>	WRF&CanESM2	WRF&CCSM4	WRF&ACCESS1–3
Average	1.4	1.8	1.6	2.1
Standard deviation	0.2	0.1	0.1	0.2
CV <sup>b</sup> %	11.3	7.8	8.5	8.6

<sup>a</sup>Gridded 10 km × 10 km precipitation interpolated by the ECCC

<sup>b</sup>Coefficient of variation

WRF agrees with ANUSPLIN data in the central and eastern MRB, but WRF tends to over-simulate the mean annual precipitation of western MRB by about 2 mm/day where the Canadian Rockies is located. These highest deviations can approach 100% in difference. The basin averaged precipitation simulated by WRF is higher than that of ANUSPLIN, with a difference ranging between 0.2 mm/day and 0.7 mm/day as shown in Table 2. The standard deviations between the simulated and the referenced data are comparable which means that the CV (coefficient of variation) of simulated precipitation is marginally smaller than the ANUSPLIN precipitation.

Based on Fig. 3 on differences between the mean MJASO (May to October) 2-m air temperature of the

observed ANUSPLIN data, and that of three GCMs down-scaled by WRF for 1979–2005, all the 2-m air temperature down-scaled by WRF agree with ANUSPLIN data, except around the Canadian Rockies at the western boundary where WRF tends to under-simulate the 2-m air temperature. Similar negative biases were reported in other studies, Fathalli et al. (2014) and Dasari et al. (2014) who found significant bias in air temperature simulated by WRF over complex topographic regions of Europe. This bias could be partly due to the terrain data used in WRF is not representative of the complex topographic feature, and the land surface interactions in the physics parametrization scheme of WRF. Further, the 2-m air temperature down-scaled by WRF using the CCSM4 data is over-simulated in eastern MRB. Other

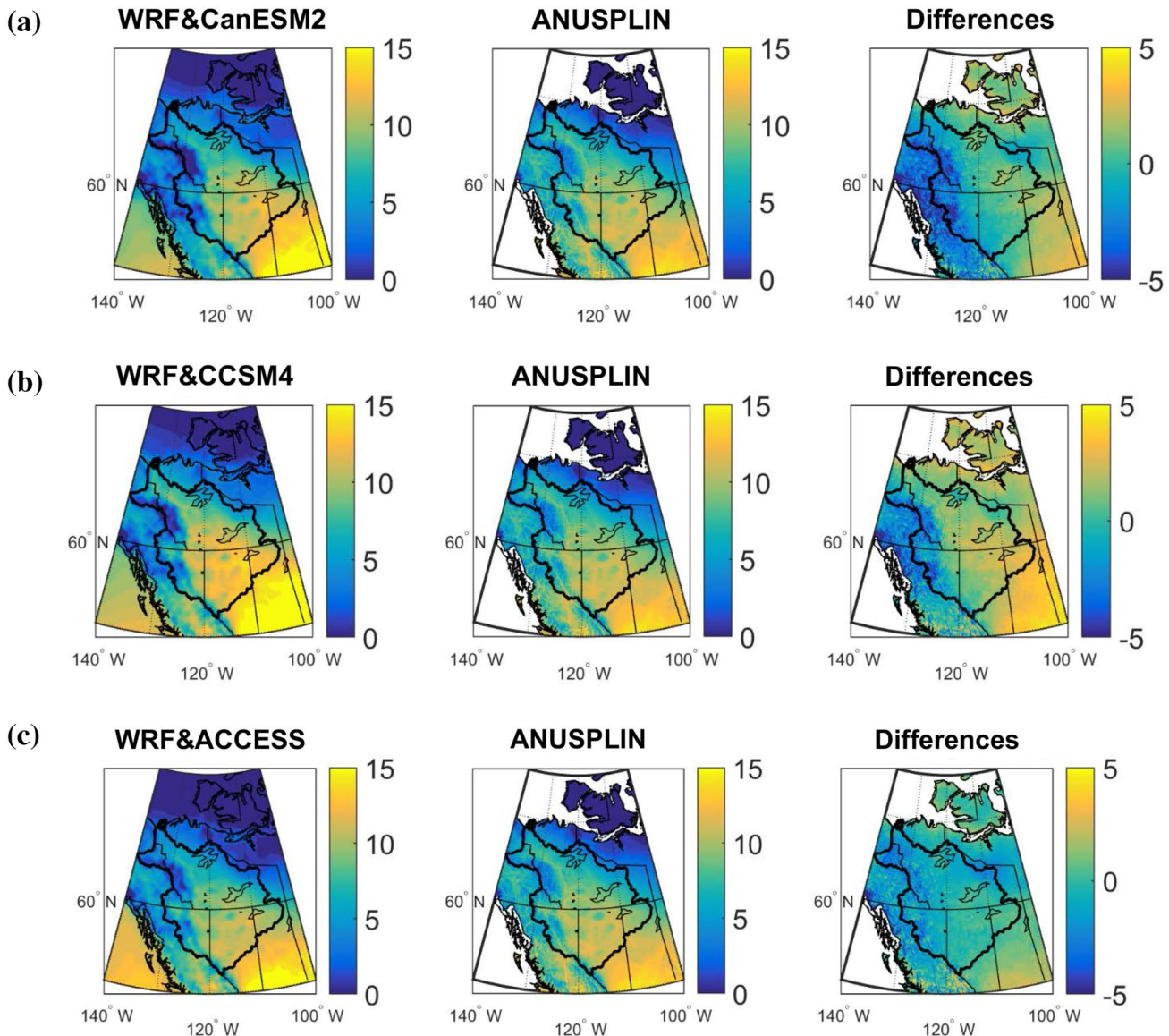


**Fig. 3** The 1979–2005 MJASO (May–October) mean air temperature ( $^{\circ}\text{C}$ ) simulated by (left) **a** WRF&CanESM2, **b** WRF&CCSM4, and **c** WRF&ACCESS, ANUSPLIN air temperature data (middle), and the differences ( $^{\circ}\text{C}$ ) between them (right)

**Table 3** Statistics of the ANUSPLIN data and the baseline air temperature (°C) downscaled by WRF at the watershed scale for MJASO

Statistics	ANUSPLIN <sup>a</sup>	WRF&CanESM2	WRF&CCSM4	WRF&ACCESS1-3
Average	8.1	7.2	8.4	7.1
Standard deviation	0.8	0.9	1.1	0.8
CV <sup>b</sup> %	9.6	12.0	13.3	10.8

<sup>a</sup>Gridded 10 km × 10 km air temperature interpolated by the ECCC<sup>b</sup>Coefficient of variation

than the bias of air temperature simulated by WRF for areas with complex terrains, the mean, standard deviation, and CV of the averaged 2-m air temperature simulated by WRF agree well with that of the reference, ANUSPLIN data as shown in Table 3.

From comparing the precipitation and 2-m temperature simulated by WRF with ANUSPLIN data over the baseline period, it is found that other than significant biases over the mountainous regions in the western boundary, discrepancies of WRF's simulations are marginal within MRB. The results demonstrate limitations of the dynamic downscaling approach by WRF at a 30-km spatial resolution in mountainous areas. A higher spatial resolution may be necessary to account for the rapid changes in rugged, mountainous terrains. However, at higher resolution, the computing resources required will be much higher under a multi-nesting domain framework.

## 4.2 Results of bias correction

### 4.2.1 Precipitation and air temperature

From Figs. 2 and 3, precipitation simulated by WRF tends to suffer over-simulation while simulated air temperature suffers under-simulation problems in mountainous areas such as the Canadian Rockies and at British Columbia near the western domain of MRB. Using the delta bias correction method (Lenderink et al. 2007), the PSS of simulated precipitation is improved from PSS = 0.11–0.56 to PSS = 0.7–0.78. Similarly, the Probability Density Function (PDF) of the bias corrected MJASO air temperature is improved from PSS = 0.59–0.69 to PSS = 0.74–0.93.

We further investigated the relationship between the delta adjusting factor and the elevation of MRB given bias is higher in the Canadian Rockies of western MRB with higher elevations (Figs. 2, 3). For simulated air temperature, delta values tend to decrease with an increase in elevation. Depending on the month and the GCM, on the basis of linear relationships

developed between elevation and the delta of air temperature, elevation can explain up to 68% of the variance (Table 4). Further, this relationship is stronger from May to July (MJ) than from August to October (ASO). However, as expected, elevation can only explain less than 10% of the variance of the bias of simulated precipitation because precipitation is much more variable spatially than air temperature which consistently decreases with elevation because of lapse rate.

The delta bias correction method can effectively adjust the simulated precipitation and air temperature so that their probability distributions agree well with that of the observed MJASO precipitation and air temperature. The good agreements with the observed data demonstrate that this bias correction method is useful at monthly to seasonal time scales. Apparently, the bias of air temperature of MJ months is also related to the effects of elevations.

### 4.2.2 Extreme precipitation indices

Bias corrected precipitation of WRF was further assessed in terms of six extreme precipitation indices to better understand the effectiveness of applying the delta bias-correction method on the extreme precipitation simulated. The spatially averaged precipitation indices were estimated from indices for each grid and the process repeated for each year across MRB. The boxplots (Fig. 4) show that the distributions obtained from ANUPLIN and that simulated by WRF are different, which was further confirmed using the Wilcoxon rank-sum test (Hollander and Wolfe 1973) at 0.05 significant level. All p-values of the test results are smaller than 0.05, which means that the null hypothesis is rejected. In terms of PSS, the highest similarity in index distributions (PSS = 0.52–0.67) between ANUSPLIN data and data simulated by WRF is CDD, while the lowest similarity in index distributions (PSS = 0.19–0.22) between the two datasets is SDII. Differences of the average between the WRF R10mm and the ANUSPLIN R10mm (PSS = 0.33–0.41) are mostly less than a day (Fig. 4a). Among

**Table 4**  $R^2$  between the delta of air temperature and the elevation

Downscaling	May	June	July	August	September	October
WRF&CanESM2	0.439	0.683	0.536	0.458	0.431	0.266
WRF&CCSM4	0.689	0.686	0.415	0.320	0.290	0.167
WRF&ACCESS1-3	0.319	0.480	0.284	0.030	0.085	0.047

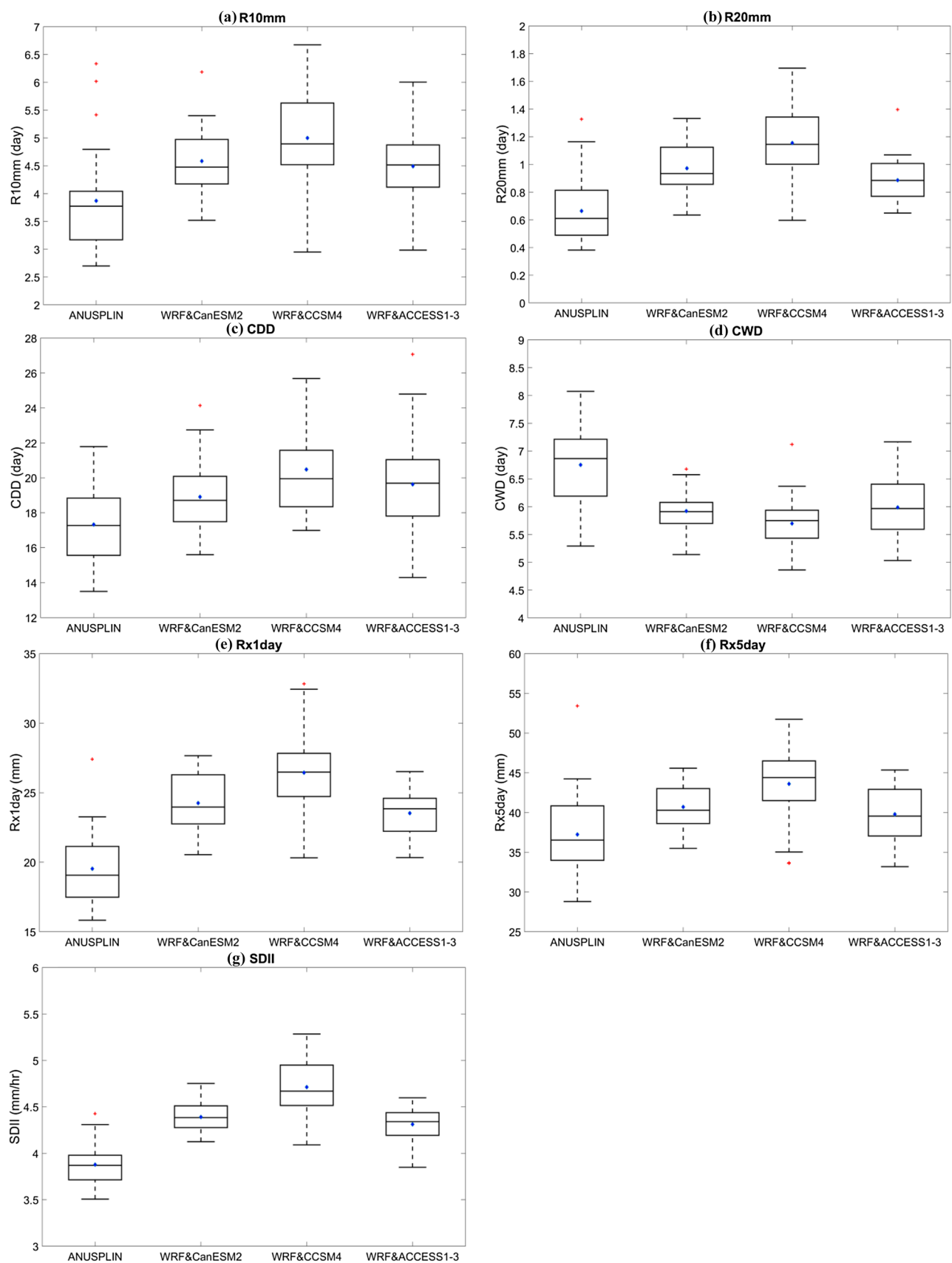


**Fig. 4** Boxplots comparing the extreme precipitation indices **a** R10mm, **b** R20mm, **c** CDD, **d** CWD, **e** Rx1day, **f** Rx5day, and **g** SDII of the baseline between the reference (ANUSPLIN) and the downscaled precipitation of WRF&CanESM2, WRF&CCSM4, and WRF&ACCESS1-3, respectively

CDD estimated from precipitation downscaled from the three GCMs, the simulated CDD is larger than the corresponding CDD of ANUSPLIN ( $PSS=0.52\text{--}0.67$ ) by about 1 to 2 days, and the simulated CWD ( $PSS=0.26\text{--}0.59$ ) is about 1 day smaller than that of ANUSPLIN (Fig. 4b, c). Differences between the averaged Rx1day of WRF and that of ANUSPLIN ( $PSS=0.22\text{--}0.33$ ) range from +5 to +7 mm, and the differences for the averaged Rx5day ( $PSS=0.33\text{--}0.63$ ) range from +4 to +8 mm (Fig. 4d, e). Differences between the averaged SDII of WRF and that of ANUSPLIN ( $PSS=0.19\text{--}0.22$ ) range from +0.4 to +0.7 mm/h.

The index distributions obtained from the ANUPLIN data and that simulated by WRF show statistical differences, but the deviations of each index in terms of PSS are relatively low to moderate. Although the delta bias correction method can

effectively adjust both the simulated MJJASO precipitation and air temperature, the performance of the delta bias correction method applied to precipitation indices is less satisfactory.

### 4.3 Projections of precipitation and temperature under climate change impact

#### 4.3.1 Projected precipitation change

The precipitation of the MRB is projected to increase marginally over 2041–2100 (Figs. 5, 6). Under the selected RCP4.5 climate scenarios, WRF simulated a marginal increase in the precipitation of MRB in the 2050 s (2041–2070) over the baseline period of 1979–2005 (Fig. 5a). The precipitation downscaled by WRF from three GCMs' RCP4.5 scenario is similar to that of the baseline period. Between 2080 s and the base period, precipitation is projected to increase marginally along the western boundary of MRB but is projected to similar precipitation amounts over other parts of MRB. Overall, under RCP4.5 climate

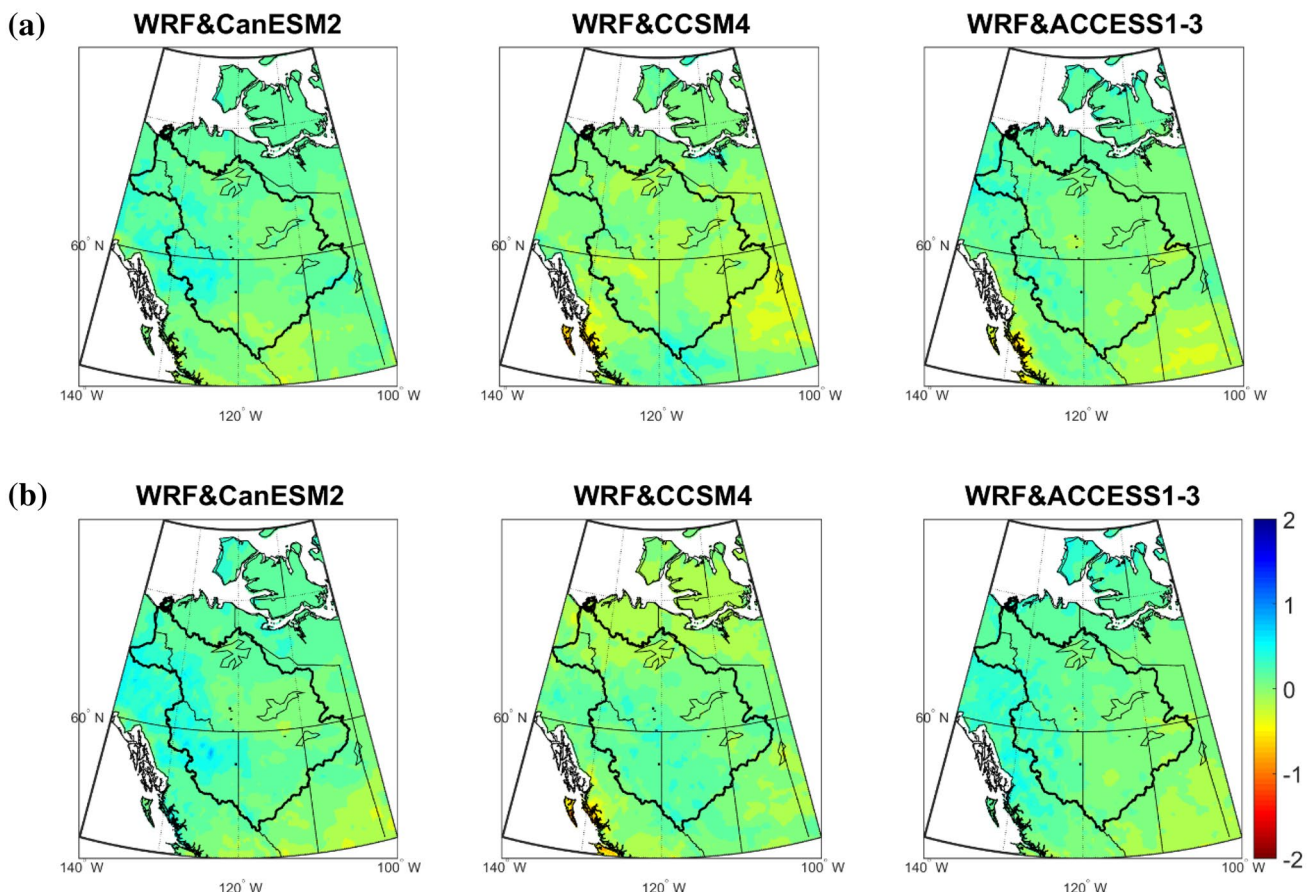


**Fig. 5** Projected mean precipitation change (mm/day) in (a) 2041–2070 and (b) 2071–2100 under RCP 4.5 climate scenarios of three GCMs downscaled by WRF

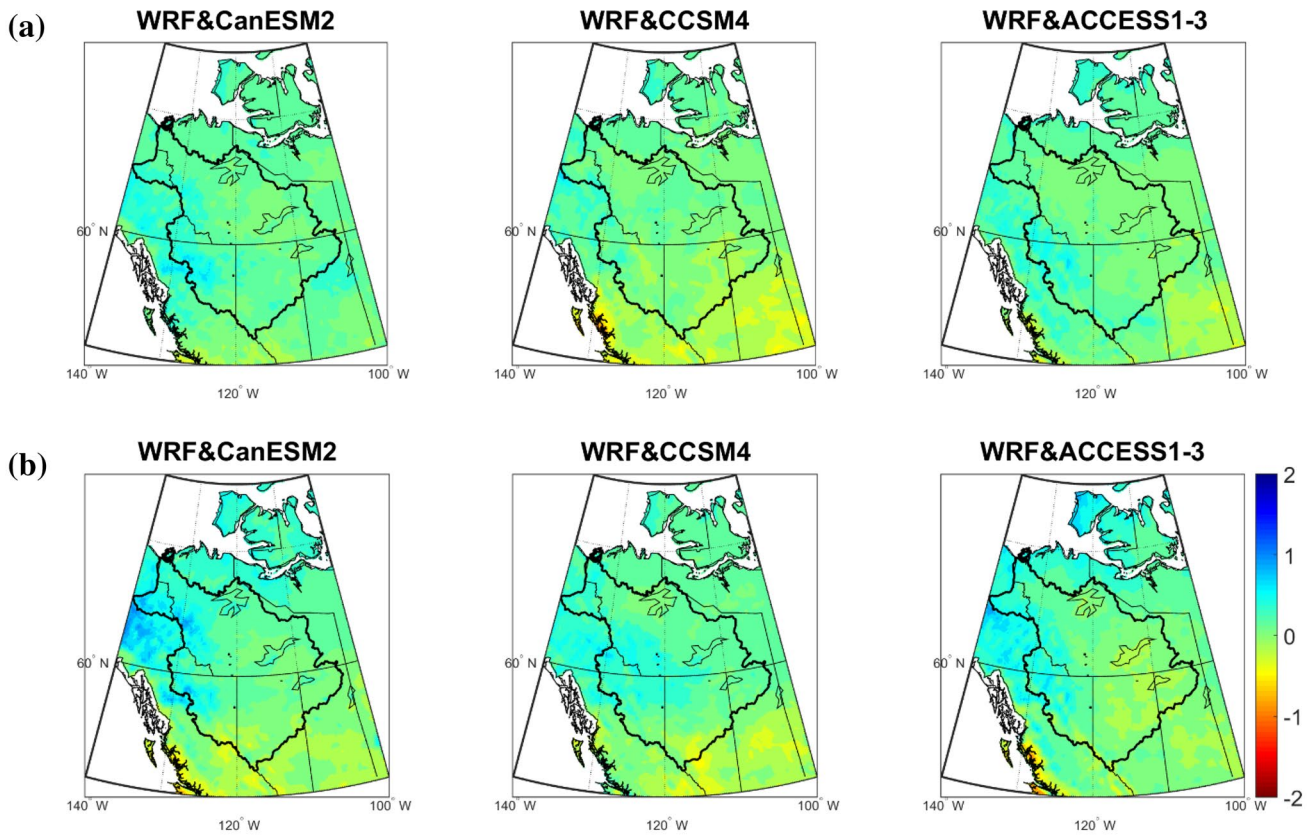


**Fig. 6** Projected mean precipitation change (mm/day) in (a) 2041–2070 and (b) 2071–2100 under RCP 8.5 climate scenarios of three GCMs downscaled by WRF

scenarios, precipitation projected for 2041–2100 is marginally higher than that of the baseline period.

Under RCP8.5 climate scenario, precipitation is projected to marginally increase in western MRB over 2041–2100. The projected increase in precipitation is higher in 2080 s than in 2050 s. Precipitation in the remaining areas of MRB is projected to similar precipitation amounts compared to the baseline period. Between RCPs 4.5 and 8.5 climate scenarios, spatial distributions of precipitation projected by WRF for MRB only differ marginally.

For the marginal changes in precipitation of MRB, most of the simulated changes in precipitation are lower than the baseline errors across MRB (Figs. 7, 8). Only the projected precipitation downscaled from CanESM2 (WRF&CanESM2) partly shows detection power ( $|P_{\text{change}}| - |P_{\text{bias}}| > 0$ ) in central and southern MRB under both RCP 4.5 and RCP 8.5 in 2041–2100.

#### 4.3.2 Projected temperature change

Compared to the baseline (1979–2005) air temperature of MRB, the spatially averaged air temperature of MRB is projected to increase consistently over the 21st Century

(Figs. 9, 10), to about 2.8 °C and 3.3 °C in 2050 s and 2080 s, respectively, under the projection of RCP 4.5 climate scenarios downscaled by WRF. The spatial distribution of 2-m air temperature increase is relatively homogenous (Fig. 9a). The southeastern MRB is projected to experience modest temperature increase of 2 °C and 3 °C in 2050 s and in 2080 s, respectively. Generally, the impact of climate change on air temperature is higher in regions of higher latitude and elevation. This is as expected because under an external forcing of, say,  $1 \text{ Wm}^{-2}$  due to the rising concentration of greenhouse gases, using the blackbody equation,  $R = \epsilon\sigma T^4$ , where  $\sigma = 5.67 \times 10^{-8} \text{ Wm}^{-2}\text{K}^{-4}$ , and assuming  $\epsilon = 1$ , it can be shown that high latitude regions of colder climate will respond to the external forcing of  $1 \text{ Wm}^{-2}$  with a larger increase in air temperature than low latitude regions of warmer climate. This is partly why Arctic amplification, climate change impact amplified in the Arctic, which has been warming at about twice the global rate since 1980 s, has been observed in recent years. The projected increasing trend in air temperature for MRB under RCP4.5 by the 2080 s is about 0.007 °C per year.

Figure 10a shows that under RCP8.5 climate scenarios, the air temperature of MRB is projected to increase between

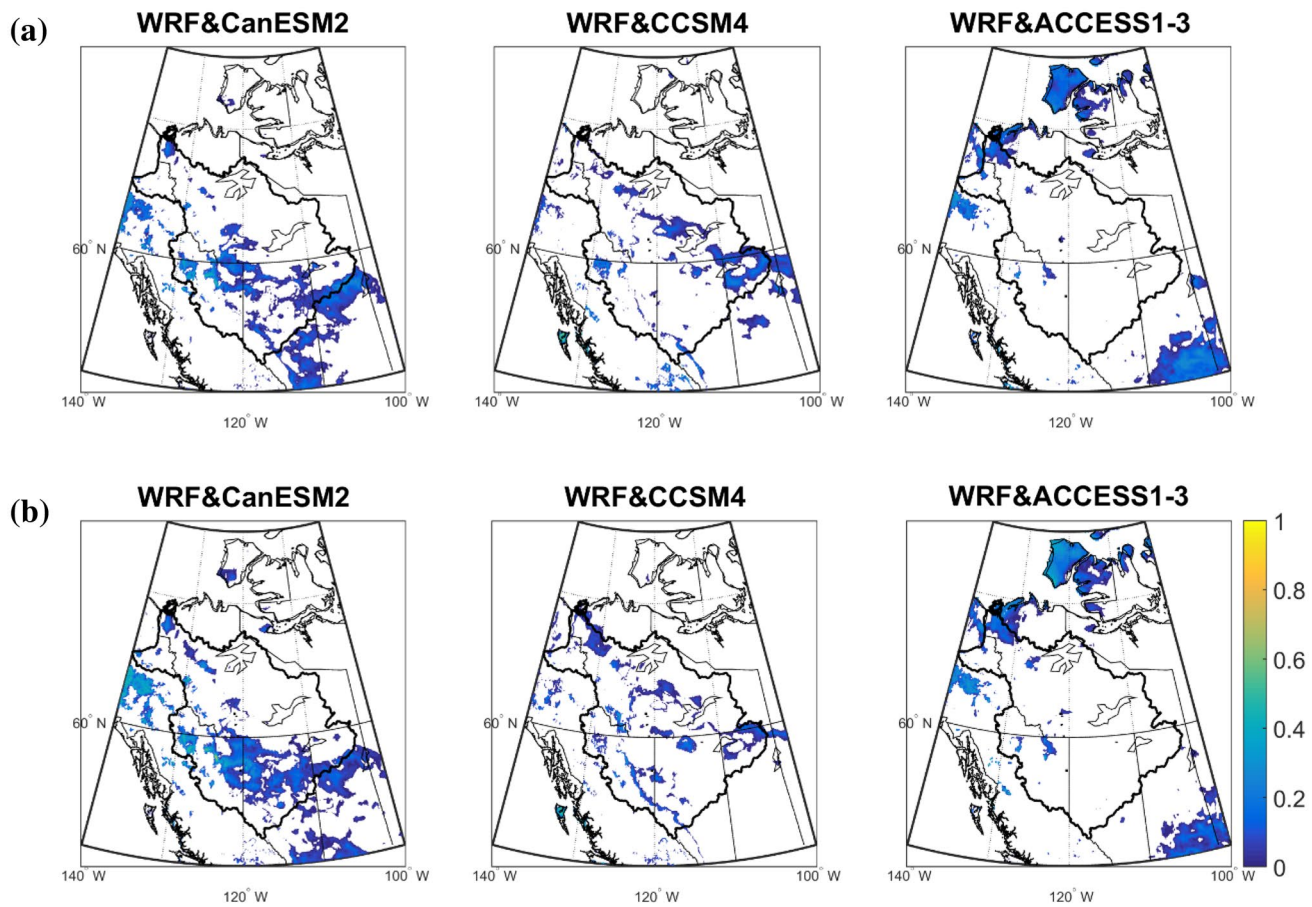


**Fig. 7** The detection power of the precipitation (mm/day) in (a) 2041–2070 and (b) 2071–2100 under RCP 4.5 climate scenarios of three GCMs downscaled by WRF. Blank colors show insufficient detection power

2 and 5 °C in 2050 s. The distribution of temperature anomaly shows moderate increase (around 2–3 °C) in the central region whereas a larger warming is projected (3–5 °C of rise) in the western and northeastern part of MRB. On the other hand, in 2080 s, based on RCP 8.5 scenarios, the spatially averaged air temperature of MRB is projected to increase from 2.5 to 6.9 °C (Fig. 10b), depending on the location of MRB. Overall, air temperature projected from downscaled RCP8.5 climate scenario of CanESM2 (WRF&CanESM2) shows the highest increase while WRF&CCSM4 (RCP8.5 of CCSM4 downscaled by WRF) projects the lowest increase in air temperature. Overall, under the RCP8.5 climate scenarios of the three GCMs downscaled by WRF, the air temperature of MRB is projected to increase significantly in 2080 s.

Most of the projected air temperature changes are higher than the baseline errors across MRB, which means that projected changes in air temperature are effectively detected, except for air temperature downscaled from CCSM4 (WRF&CCSM4) under RCP 4.5 in 2041–2100, and in western and eastern MRB (see light colors in the middle column of Fig. 11a, b). Similarly, projected air temperature

downscaled from CCSM4 (WRF&CCSM4) under RCP 8.5 in 2041–2070 are also not higher than the baseline error in western MRB. Similar changes in the spatial pattern of air temperature are simulated by WRF for CanESM2 scenarios under RCP4.5 for 2041–2100 and under RCP8.5 for 2041–2070.

The detection powers by WRF are about 2–3 °C across MRB (Figs. 11, 12), but that for CanESM2 and CCSM4 increase to 4–7 °C across MRB under RCP 8.5 for 2071–2100 (the left and right columns of Fig. 12b), and it is the highest in central MRB. The detection power method is a useful tool to confirm the projected changes in air temperature by WRF after bias correction with high confidence.

#### 4.4 The uncertainty of future projections of the extreme precipitation indices

Boxplots of the projected six extreme precipitation indices, R10mm, CDD, CWD, Rx1day, Rx5day, and SDII are shown in Fig. 13. The average of all projected changes in R10mm in 2050 s and 2080 s (2041–2070 and 2071–2100)

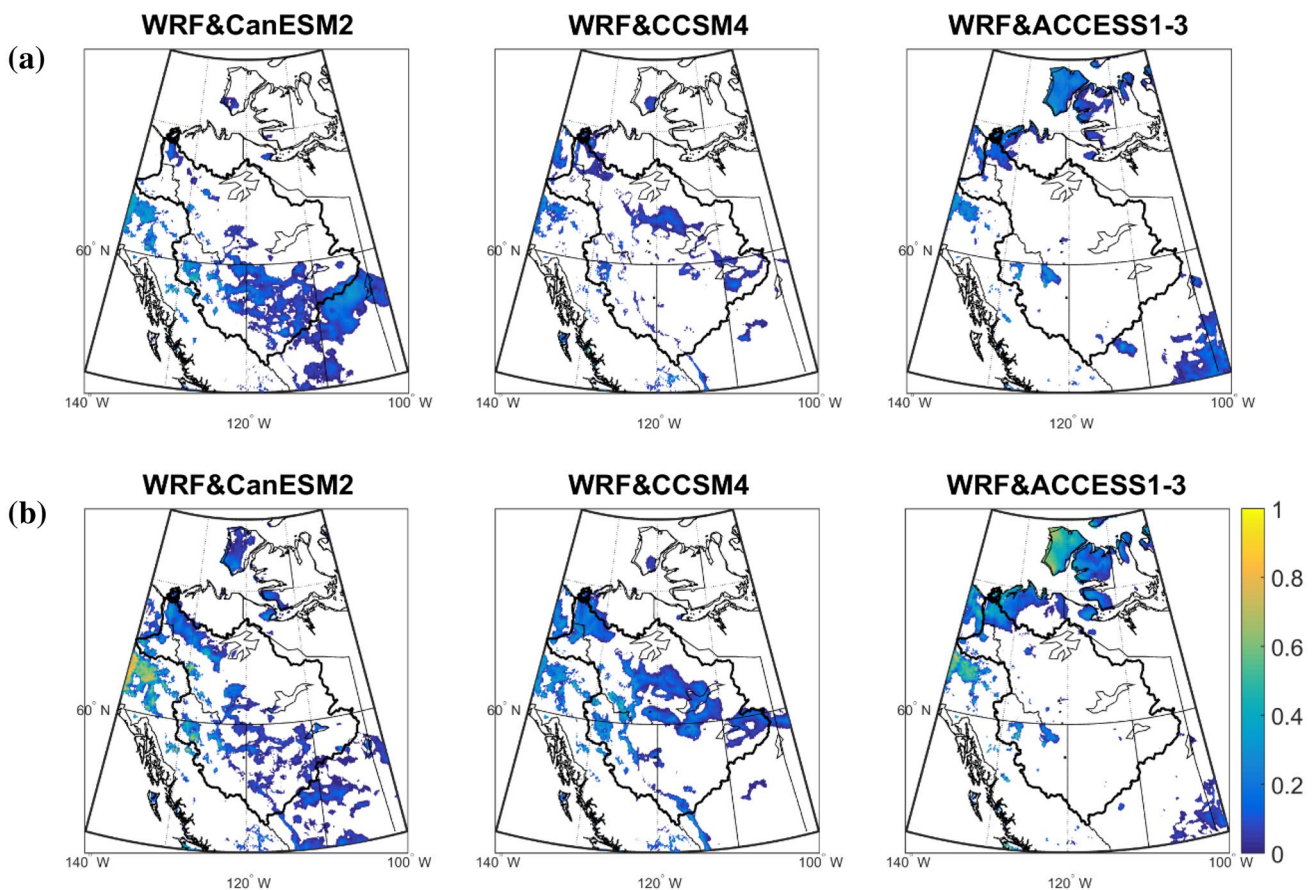


**Fig. 8** The detection power of the precipitation (mm/day) in (a) 2041–2070 and (b) 2071–2100 under RCP 8.5 climate scenarios of three GCMs downscaled by WRF. Blank colors show insufficient detection power

under both RCP4.5 and RCP8.5 climate scenarios is modest at about 18% ( $-2.1\%$  to  $+32.8\%$ ) (Fig. 13a). Among all the projected changes for R10mm, WRF-CanESM2 and WRF-ACCESS1-3 project a 50% change which is higher than the baseline percentage errors (Blue dash lines in Fig. 13a), which means that R10mm would likely increase in 2041–2100.

The maximum number of consecutive dry and wet days (CDD and CWD) are projected to remain similar between the baseline period and 2041–2100 under both RCP4.5 and RCP8.5 climate scenarios (Fig. 13b, c). The range of the projected CDD is higher in the 2080 s than the 2050 s, which is expected given uncertainty grows as we project to the distant future. Since most of these changes are within the baseline percentage errors, the projected changes in CDD and CWD are less certain compared to precipitation indices such as R10mm and others.

The annual maximum daily and 5-day precipitation (Rx1day and Rx5day) for MJJASO are both projected to increase in 2041–2100 under both RCP4.5 and RCP8.5 climate scenarios. The projected change ranges from  $-0.93$  to  $11.65\%$  with an average of  $6.1\%$ , and from  $0.53$  to  $16.02\%$

with an average of  $9.4\%$ , for Rx1day and Rx5day, respectively. As the baseline percentage errors of Rx1day are high, projected changes in Rx1day are less certain. On the other hand, WRF-CanESM2 and WRF-ACCESS1-3 project a 50% change in Rx5day which is higher than the baseline percentage errors (Fig. 13e), which means that Rx5day will likely increase in 2041–2100 under both RCP4.5 and RCP8.5 climate scenarios. In addition, nine out of the twelve first quartiles (25th percentile) of the Rx5day boxplots are above the baseline average (Fig. 13e).

On average, the simple precipitation intensity index (SDII) is projected to increase by 2.4 to  $9.4\%$  in the 2050 s and 2.6 to  $12.9\%$  in the 2080 s under both RCP4.5 and RCP8.5 climate scenarios. The projected increase for SDII ranges from 8.9 to  $12.9\%$  in the 2080 s under RCP8.5 climate scenarios, and WRF-CanESM2 and WRF-ACCESS1-3 project changes that are 50% higher than the baseline percentage errors, which means that precipitation intensities will likely increase in the 2080 s under RCP8.5 climate scenarios. Overall, ten out of the 12 first quartiles (25th percentile) of the SDII boxplots are above the baseline average of SDII (Fig. 13f). The high projected increases for SDII is

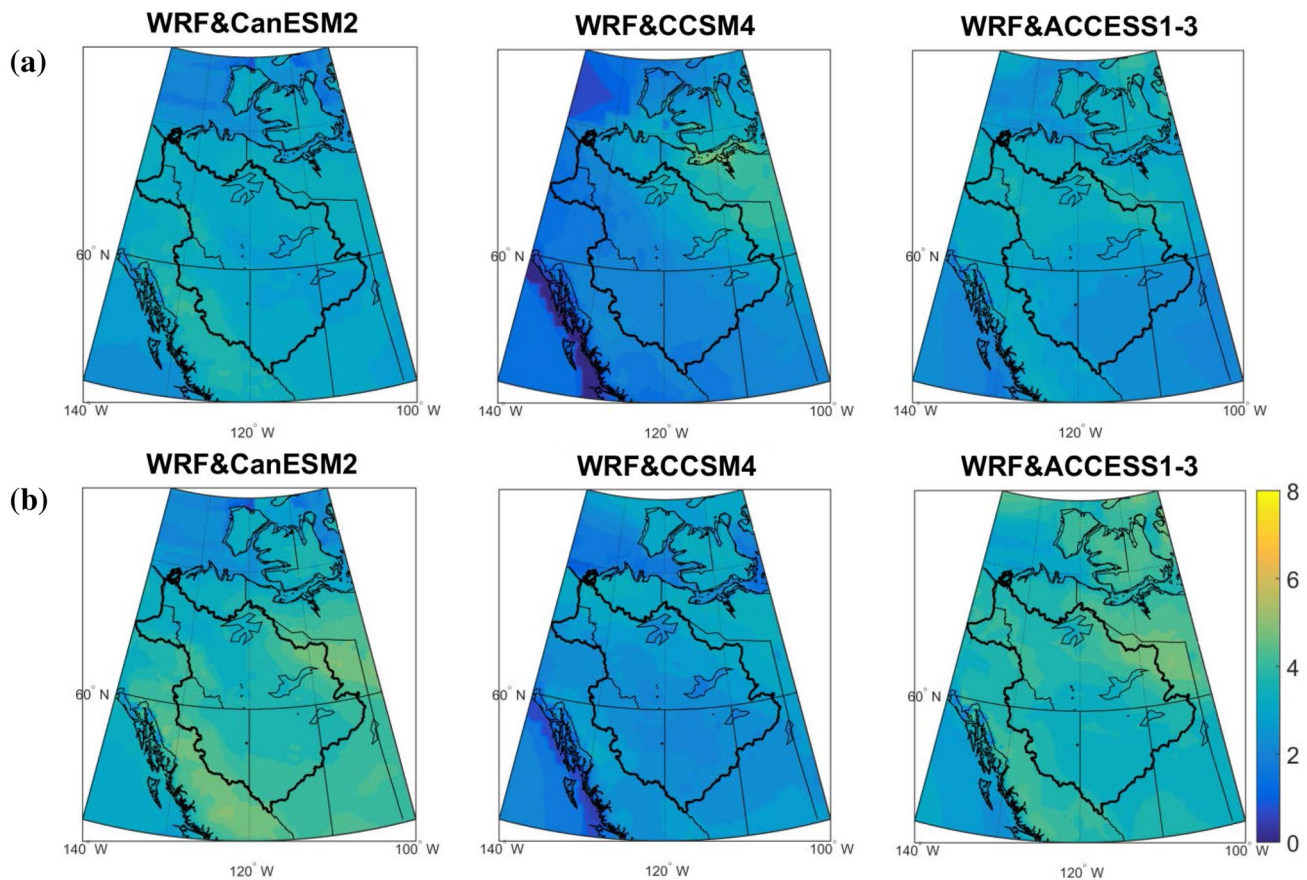


**Fig. 9** Projected mean surface air temperature change ( $^{\circ}\text{C}$ ) in (a) 2041–2070 and (b) 2071–2100 under RCP 4.5 climate scenarios of three GCMs downscaled by WRF

in 2080 s under the downscaled RCP8.5 climate scenario of CanESM2 and ACCESS1-3, which also projected substantial warming in MRB in 2080 s (Fig. 14a).

The detection power approach can also effectively identify the degree of projected changes in extreme precipitation indices of MRB, e.g., R10mm and Rx5day are expected to change substantially in 2041–2100. Apparently, the results show that WRF-CanESM2 and WRF-ACCESS1-3 can better project changes to the precipitation of MRB.

#### 4.5 Projected changes in spatially averaged air temperature and precipitable water

The rising concentration of greenhouse gases leads to climate warming (IPCC 2007, 2013), which, according to the Clausius–Clapeyron relation, increases the atmospheric moisture-holding capacity approximately by  $7\%/\text{ }^{\circ}\text{C}$ . As a result, the atmosphere can accommodate more precipitable water, resulting in more evaporation and more precipitation (Houghton 2007). The rainfall amount was projected to increase by  $1\%/\text{K}$  and the distribution shifts by  $3.3\%/\text{K}$  based on the CMIP5 (Coupled Model Intercomparison Project 5)

simulations to  $\text{CO}_2$  doubling (Pendergrass and Hartmann 2014). In other words, global warming can potentially cause future extreme storm events to occur more frequently and in greater severity. Therefore, in this section, we will discuss how precipitable water will change in response to temperature change.

Figure 14a shows spatially averaged, 2-m annual air temperature anomaly time series for MRB based on the RCP4.5 and RCP8.5 climate scenarios dynamically downscaled by WRF. Shaded blue and red plots represent the range of air temperature projected by WRF driven by RCP4.5 and RCP8.5 climate scenarios of three GCMs, respectively. The spatially averaged, air temperature anomaly time series simulated shows consistent increasing trends, which imply that MRB is expected to experience gradual warming from 2041 to 2100. The projected increasing trends in air temperature for MRB estimated from the Theil-Sen estimator (Sen 1968) ranges between  $0.0004\text{ }^{\circ}\text{C}/\text{year}$  and  $0.027\text{ }^{\circ}\text{C}/\text{year}$  under RCP4.5 climate scenarios, and between  $0.05\text{ }^{\circ}\text{C}/\text{year}$  and  $0.086\text{ }^{\circ}\text{C}/\text{year}$  under RCP8.5 climate scenarios. Initially, under RCP4.5 and RCP8.5 climate scenarios, WRF projects a similar range of temperature increase in MRB in

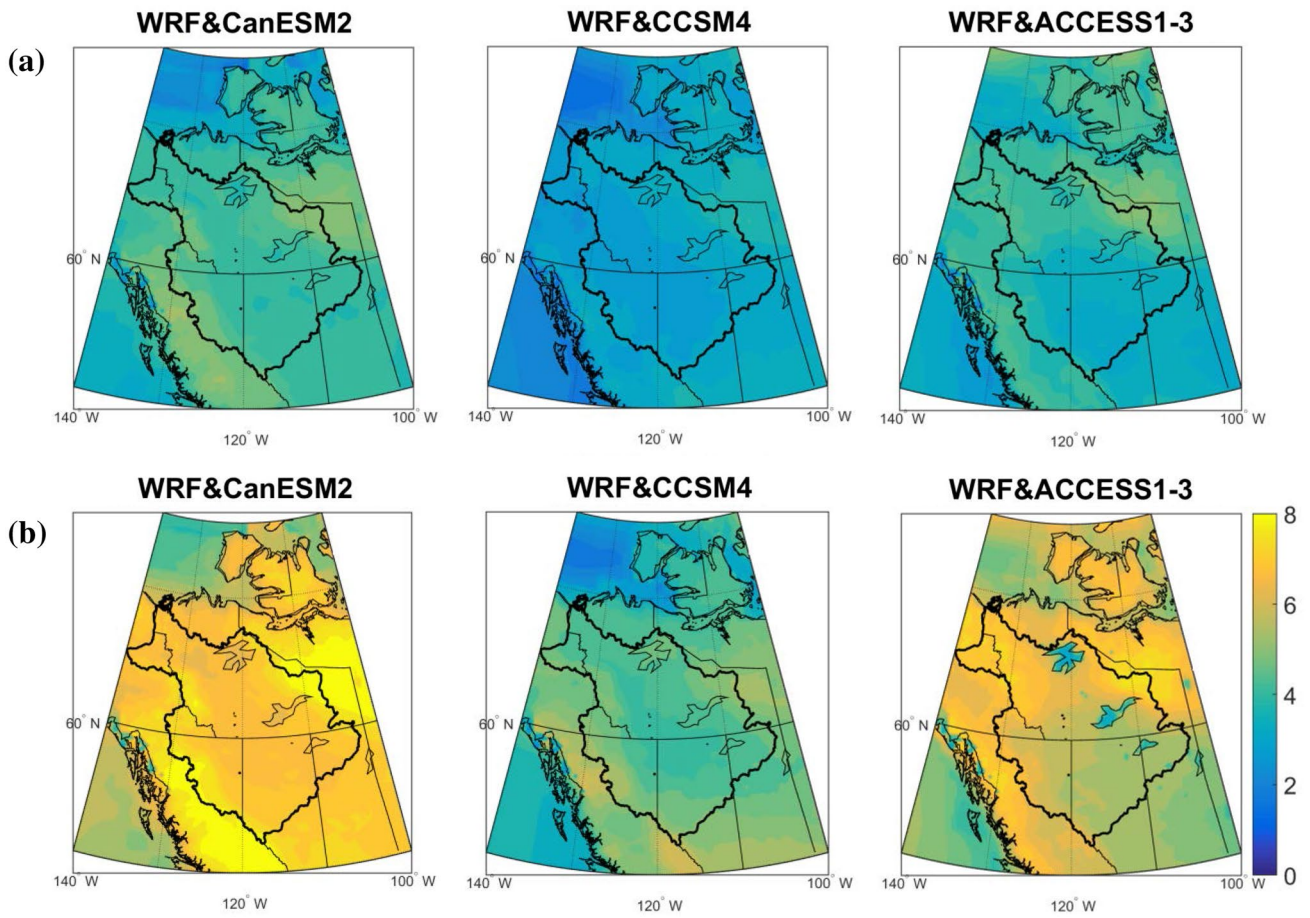


**Fig. 10** Projected mean surface air temperature change ( $^{\circ}\text{C}$ ) in (a) 2041–2070 and (b) 2071–2100 under RCP 8.5 climate scenarios of three GCMs downscaled by WRF

2050 s, but by 2080 s, WRF projects a higher increase in air temperature in MRB under RCP8.5 than under RCP4.5 scenarios. Based on the Mann–Kendall test at a 0.05 significance level, other than the 2-m air temperature anomaly based on the RCP4.5 climate scenario of WRF&CCSM4, the trend of the 2-m air temperature anomaly time series in 2041–2100 are all statistically significant for RCP4.5 and RCP8.5 climate scenarios.

Precipitable water is a depth of water vapour integrated over the entire column of the atmosphere. The spatially averaged, precipitable water annual anomaly time series for the MJASO season simulated by WRF for RCP4.5 and RCP 8.5 climate scenarios also consistently show increasing trends similar to the projected 2-m air temperature. In Fig. 14b, the shaded colors represent the range of projected precipitable water change (%) for both dynamically downscaled RCP scenarios using initial and lateral boundary conditions of the three GCMs. The projected increasing trend in precipitable water ranges between 0.085%/year and 0.254%/year under RCP4.5 climate scenarios, and between 0.486%/year and 0.718%/year under RCP8.5 climate scenarios. Under

both climate scenarios, the projected increase in precipitable water ranges from about 9.4–43.2% with an average of 22.5% in the 2050 s, and about 11.9% to 64.7% with an average of 34.5% in the 2080 s.

In MRB, a marginally higher range of precipitable water increase is projected under RCP 8.5 than under RCP4.5 climate scenario in 2050 s. However, in 2080 s, a significantly higher increase in precipitable water in MRB is projected under RCP8.5 than under RCP4.5 scenarios, with an average projected increase of about 45.8% and about 23.3%, respectively. Overall, based on the Mann–Kendall's test at a 0.05 significance level, the increasing trends of precipitable water over 2041–2100 are statistically significant.

Both air temperature and precipitable water are projected to increase in 2041–2100. However, other than R10mm and Rx5day, the higher air temperature and precipitable water projected do not result in obvious changes in other precipitation indices because the characteristics of seasonal precipitation also depend on other climatic factors.

Kurkute et al. (2019) used a high resolution convection permitting (CP) of WRF, Version 3.6.1, a horizontal

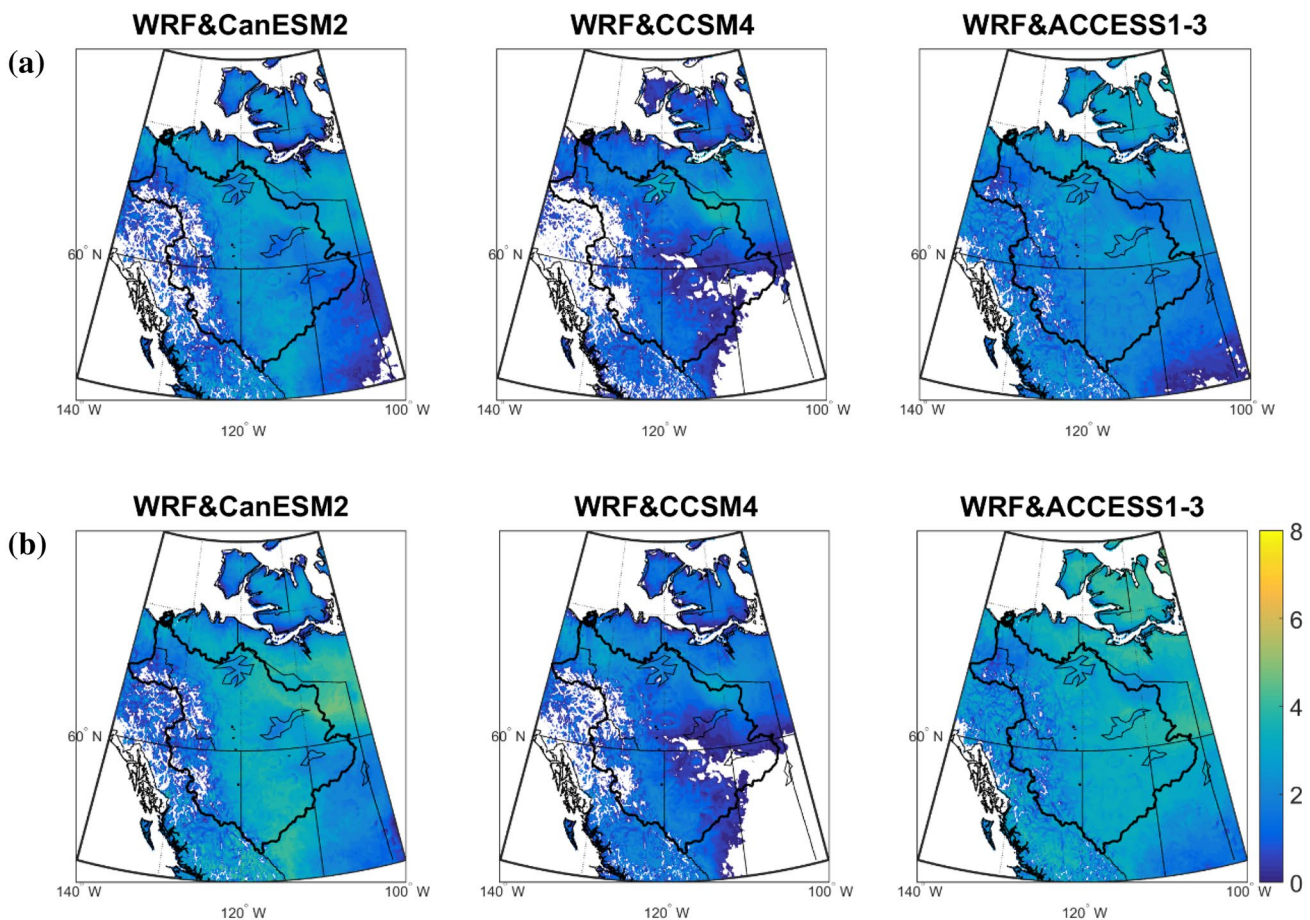


**Fig. 11** The detection power of the air temperature ( $^{\circ}\text{C}$ ) in (a) 2041–2070 and (b) 2071–2100 under RCP 4.5 climate scenarios of three GCMs downscaled by WRF. Blank colors show insufficient detection power

resolution of 4 km, and 37 vertical Eta levels with the model top at 50 hPa. They used the New Thompson micro-physics scheme, the Yonsei University (YSU) scheme for PBL, the short-wave and long-wave radiations of CAM schemes, and the Noah land surface model. With a 4-km horizontal resolution, the model explicitly resolves deep convections, and the deep cumulus parameterization was turned off. They investigated the surface water budget and atmospheric moisture balance in historical and RCP8.5 projections by comparing the results with three reanalysis datasets: NARR (32 km), JRA-55 (55 km), and ERA-Interim (79 km). As expected, they found the High-resolution WRF out-performs the reanalyses in balancing the surface water budget in MRB with much lower residual terms. For the global warming scenario at the end of the 21st century with RCP8.5 radiative forcing, MRB is projected to increase in precipitation and evapotranspiration but a decrease in runoff. Despite of the difference in resolution (4-km versus 30-km), and different versions and configurations of WRF, our results on the projected changes of MRB based on downscaled climate scenarios

of three GCMs of CMIP5 by WRF at 30-km resolution are similar to that of Kurkute et al. (2019).

## 5 Conclusions and recommendations

This study investigated the potential impact of climate warming on changes to the regional climate of MRB by the dynamic downscaling method of a regional climate model, WRF. The results obtained at a higher spatial resolution (30-km) than those of GCMs provide us a clearer picture of the future regional climate of MRB for 2041–2100 under the potential impact of RCP4.5 and RCP8.5 climate scenarios. The detection power approach was applied to projected changes in air temperature, precipitation, and six extreme precipitation indices investigated in this study. The results obtained from dynamically downscaled and bias corrected precipitation and temperature data for MRB demonstrate the expected regional warming and changes in precipitation (R10mm and Rx5day) in 2041–2100.

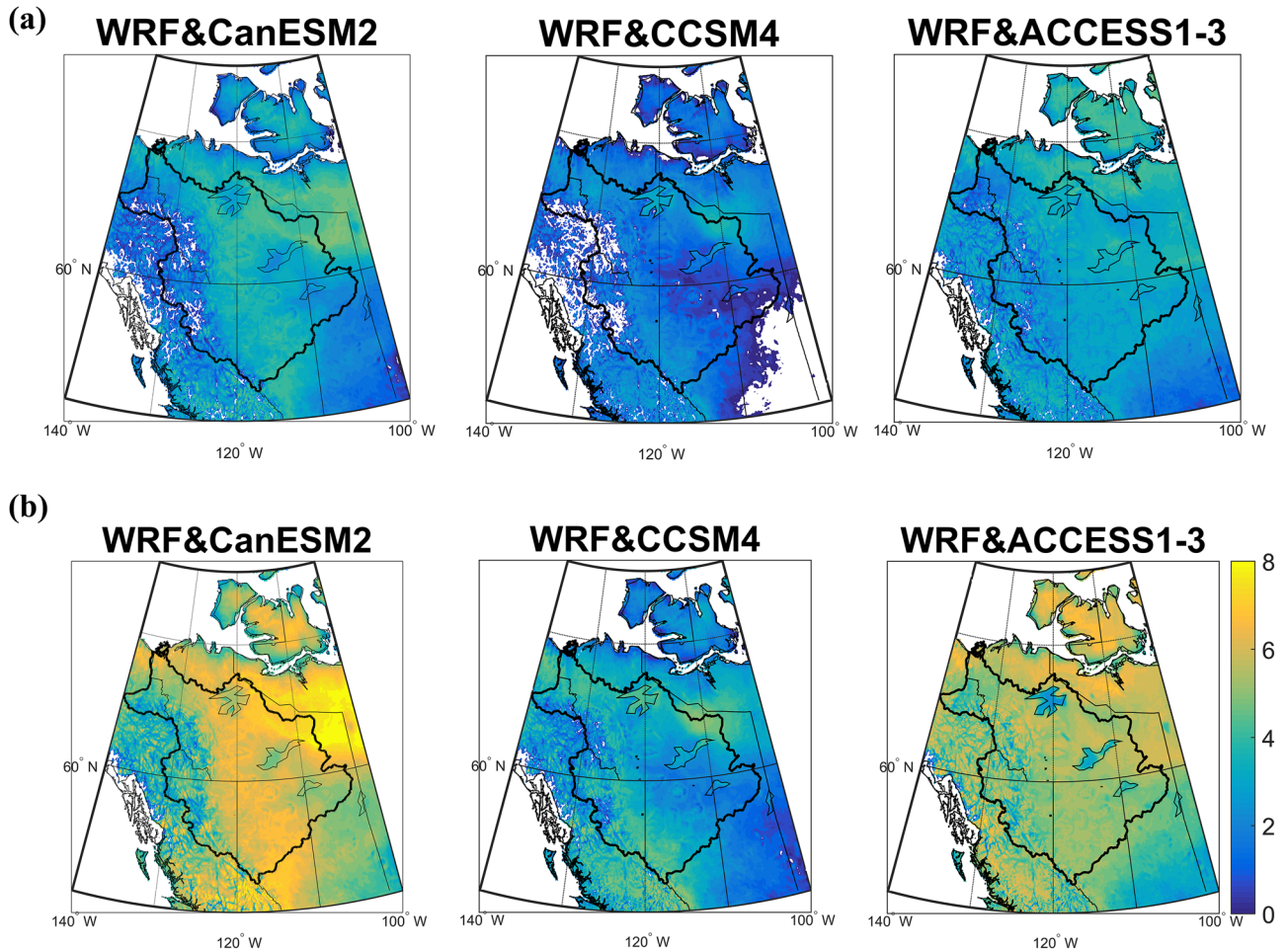


**Fig. 12** The detection power of the air temperature ( $^{\circ}\text{C}$ ) in (a) 2041–2070 and (b) 2071–2100 under RCP 8.5 climate scenarios of three GCMs downscaled by WRF. Blank colors show insufficient detection power

Air temperature downscaled by WRF from GCMs' data for the historical period shows a good agreement with the ANUSPLIN data except air temperature in the Canadian Rockies is mostly under-simulated partly because rugged terrains of the Rockies are not well represented in WRF. Precipitation downscaled by WRF from the GCMs' data agrees with the ANUSPLIN precipitation data except positive bias is detected in the Canadian Rockies.

From RCP4.5 climate scenarios of the three GCMs downscaled by WRF for the projected periods of 2041–2100, air temperature of MRB is projected to consistently increase by 2.5 to 3.8  $^{\circ}\text{C}$  in the MJASO season of 2080 s over the baseline (1979–2005) period. Generally, climate change is projected to increase the air temperature marginally higher in colder regions of MRB with higher latitudes and elevations. Spatially, the western MRB is projected to experience higher temperature rise than the central MRB. However, projected changes in air temperature in western MRB under RCP 4.5 climate scenarios are

modest. However, from RCP8.5 climate scenarios of the three GCMs downscaled by WRF, air temperature of MRB are projected to increase both in 2050 s and in 2080 s by 4.5–6.9  $^{\circ}\text{C}$ , respectively. Warming is projected to be more pronounced around the boundary of MRB, while central MRB would experience a more modest increase in air temperature.

Based on RCP 8.5 and RCP4.5 climate scenarios of the three GCMs downscaled by WRF, precipitation of MRB is projected to marginally increases in the 2050 s and 2080 s. Spatially, precipitation can increase in middle MRB and in the Canadian Rockies, but only marginal changes are projected in other parts of MRB. The detection power of precipitation changes is low for most of the MRB under both climate scenarios.

Despite of uncertainties associated with long-term projections under the impacts of climate change, MRB will likely experience warming in the 2050 s and 2080 s under the climate scenarios of RCP4.5 and RCP8.5. Given

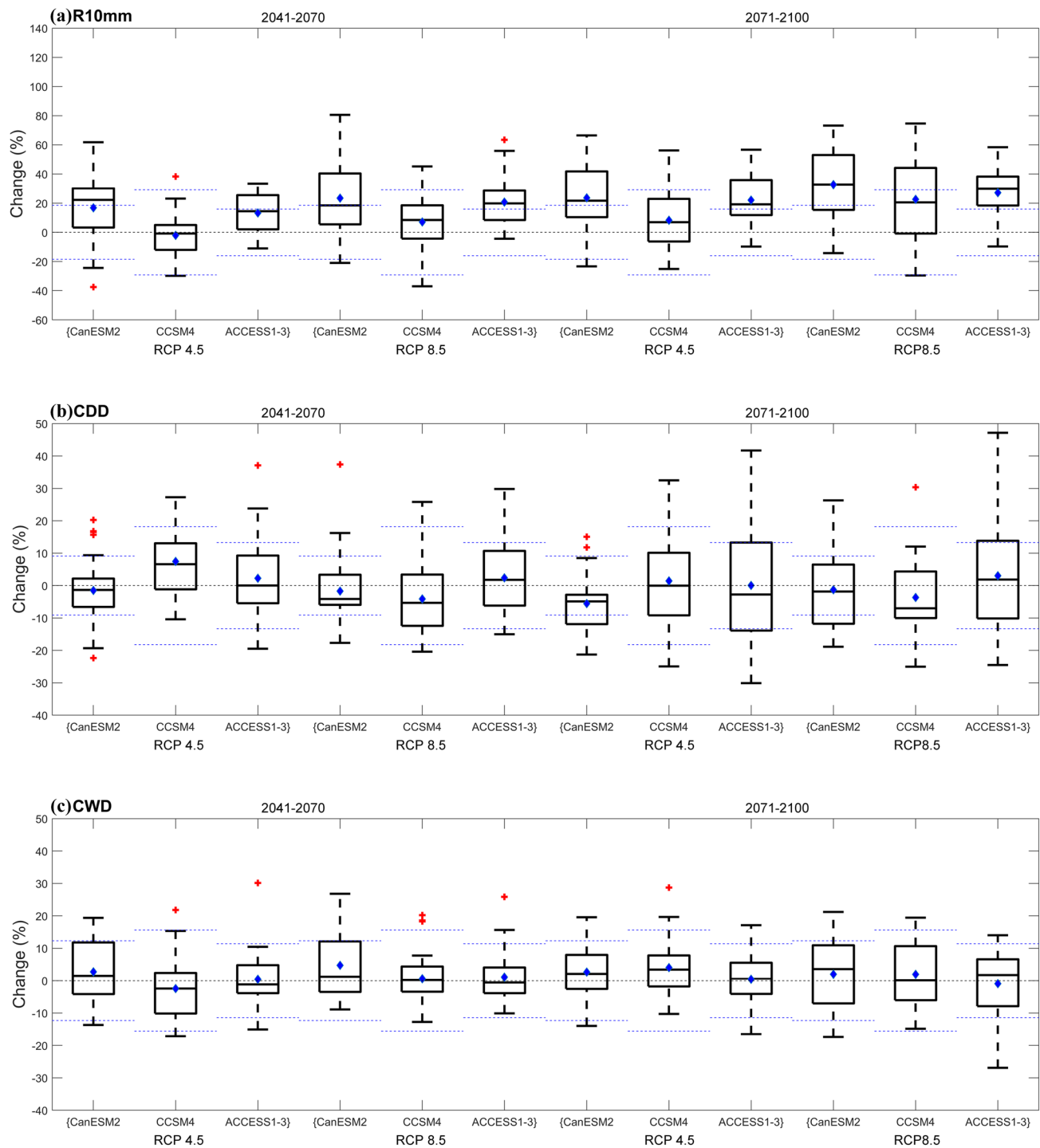


**Fig. 13** Boxplots of changes of six precipitation indices downscaled from CanESM2, CCSM4, and ACCESS1-3 models in 2041–2070 and 2071–2100 under RCP 4.5 and RCP 8.5 climate scenarios. The

red crosses are the outliers and the blue rhombuses are averages as defined in Fig. 4. The blue dash lines are the baseline percentage errors

the four extreme precipitation indices (R10mm, Rx1day, Rx5day, and SDII) show increasing trends. Among these, R10mm and Rx5day have higher detection power in

changes. It seems that future extreme precipitation events will become more severe, even though the water level of the Mackenzie River is projected to decrease in 2041–2100

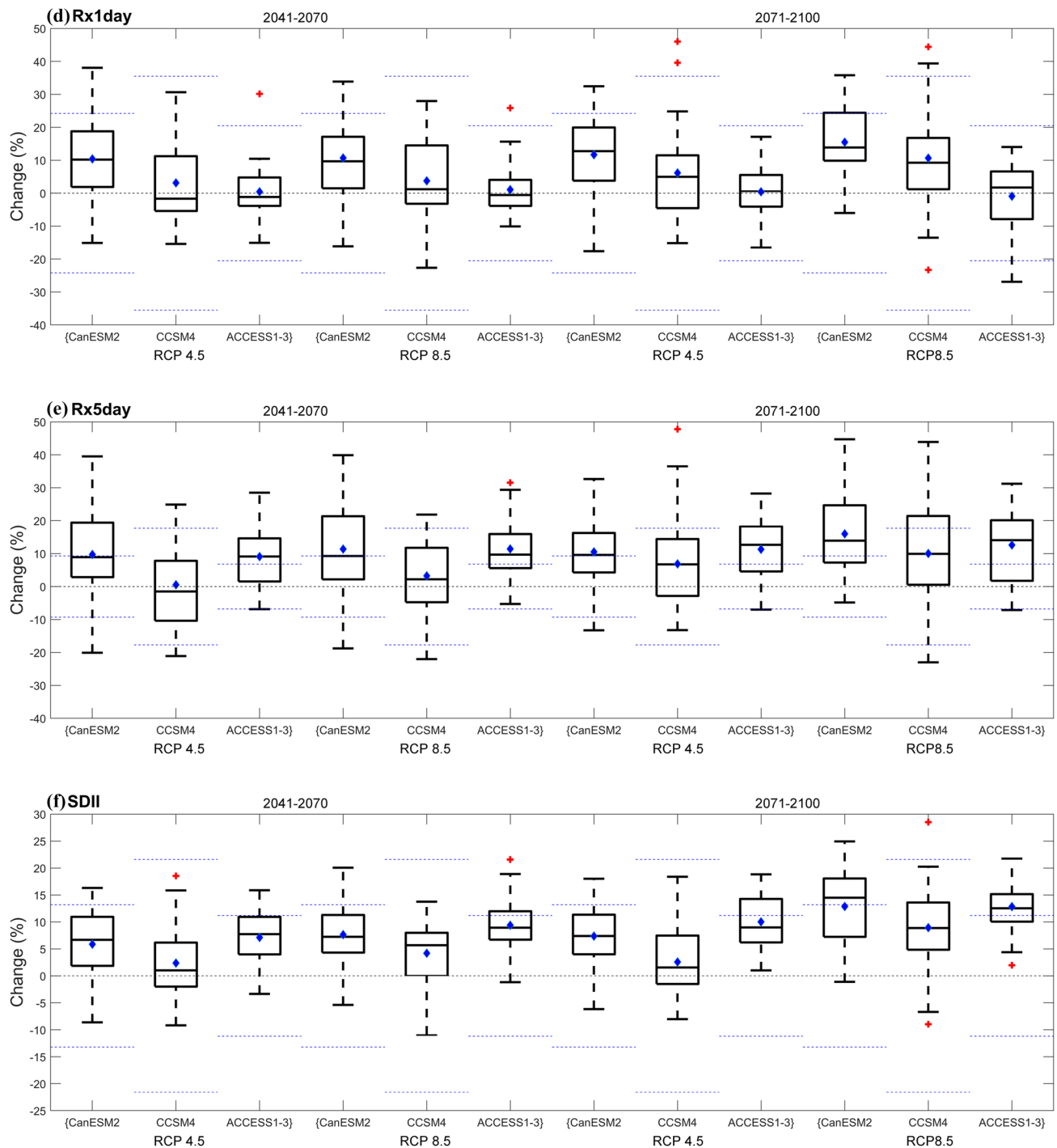


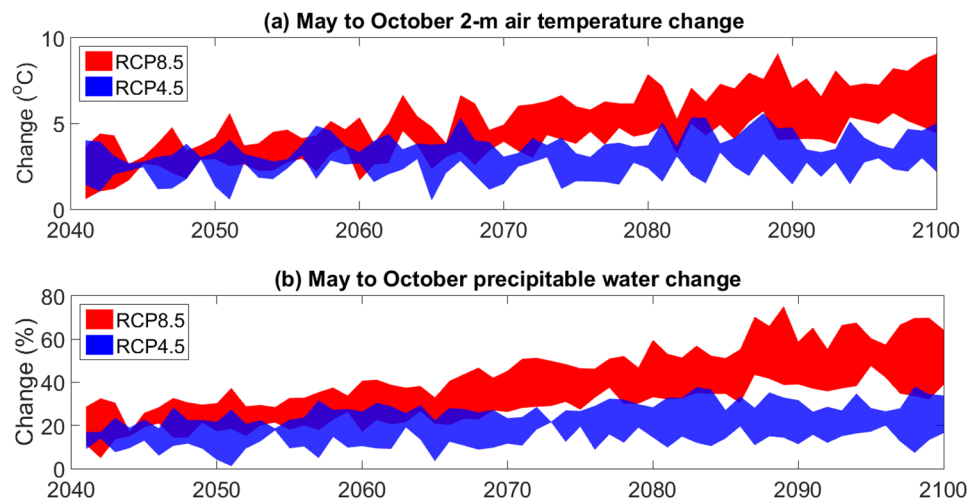
**Fig. 13** (continued)

(Scheepers et al. 2018). It seems that global warming will affect the water resources, ecosystems, and the inland waterway transportation of MRB. Large scale studies on the possible impacts of climate change and adaptive measures to mitigate the potential impact of climate change to the water balance, ecosystems, biodiversity, and inland

waterways of MRB should be conducted, similar to the Mackenzie GEWEX study conducted in 1995–2005, e.g., Stewart et al. (1998).

We have focused on the potential impact of climate change on air temperature, precipitation, and precipitation indices in the Mackenzie River Basin (MRB) for summer

**Fig. 14** Changes of (a) the air temperature and (b) precipitable water downscaled from CanESM2, CCSM4, and ACCESS1-3 models in the 2041–2100 under RCP 4.5 and 8.5 scenarios



and fall seasons. However, the impact to the winter season is also important because the Northern Canada is expected to experience higher warming than other parts of Canada, especially in winters (Government of Canada 2019). Therefore, future investigations should focus on the impact to winter snowfall, snow water equivalent, and the onset of spring snowmelt within MRB because spring snowmelt runoff represent a major component of the streamflow of MRB. Furthermore, more bias correction methods should be investigated in the bias correction of climate variables dynamically downscaled by a regional climate model (e.g., Cannon 2018) for regional climate change studies.

**Acknowledgements** This study was funded by Transport Canada under the Northern Transport Adaptation Initiative (NTAI) program. The ANUSPLIN, NARR data, GCM climate scenarios data of CMIP5 and ERA-Interim reanalysis data, etc., were downloaded from the websites of Environment Canada NCEP, ESGF and ECMWF, respectively. Supercomputing resources of this study was provided by Compute Canada's WestGrid supercomputing program. The regional climate model, WRF (Weather Research and Forecasting), was downloaded from the website of wrf-model.org. The study was funded by Natural Sciences and Engineering Research Council of Canada under NSERC.

## References

- Al Aamery N, Fox JF, Snyder M (2016) Evaluation of climate modeling factors impacting the variance of streamflow. *J Hydrol* 542:125–142. <https://doi.org/10.1016/j.jhydrol.2016.08.054>
- Arora VK, Scinocca JF, Boer GJ, Christian JR, Denman KL, Flato GM, Kharin VV, Lee WG, Merryfield WJ (2011) Carbon emission limits required to satisfy future representative concentration pathways of greenhouse gases. *Geophys Res Lett*. <https://doi.org/10.1029/2010gl046270>
- Aziz OIA, Burn DH (2006) Trends and variability in the hydrological regime of the Mackenzie River Basin. *J Hydrol* 319:282–294. <https://doi.org/10.1016/j.jhydrol.2005.06.039>
- Bawden AJ, Linton HC, Burn DH, Prowse TD (2014) A spatiotemporal analysis of hydrological trends and variability in the Athabasca River region, Canada. *J Hydrol* 509:333–342. <https://doi.org/10.1016/j.jhydrol.2013.11.051>
- Beltos S (ed) (2008) River ice breakup. Water Resources Publications, Highlands Ranch, p 462
- Brabets TP, Walvoord MA (2009) Trends in streamflow in the Yukon River Basin from 1944 to 2005 and the influence of the Pacific Decadal Oscillation. *J Hydrol* 371:108–119. <https://doi.org/10.1016/j.jhydrol.2009.03.018>
- Burn DH (2008) Climatic influences on streamflow timing in the headwaters of the Mackenzie River Basin. *J Hydrol* 352:225–238. <https://doi.org/10.1016/j.jhydrol.2008.01.019>
- Cannon AJ (2018) Multivariate quantile mapping bias correction: an N-dimensional probability density function transform for climate model simulations of multiple variables. *Clim Dyn* 50:31–49. <https://doi.org/10.1007/s00382-017-3580-6>
- Collins WD, Rasch PJ, Boville BA, Hack JJ, McCaa JR, Williamson DL, Kiehl JT, Briegleb B, Bitz C, Lin SJ, Zhang M, Dai Y (2004) Description of the NCAR community atmosphere model (CAM3.0). Boulder: NCAR. NCAR technical note TN-4641STR, 214 pp
- CSIRO and Bureau of Meteorology (2015) Climate change in australia technical report, Melbourne, Australia. [www.climatechangeinaustralia.gov.au](http://www.climatechangeinaustralia.gov.au)
- Dasari HP, Salgado R, Perdigao J, Challa VS (2014) A regional climate simulation study using WRF-ARW model over Europe and evaluation for extreme temperature weather events. *Int J Atmos Sci* 2014
- de Queiroz AR, Lima LMM, Lima JWM, da Silva BC, Scianni LA (2016) Climate change impacts in the energy supply of the Brazilian hydro-dominant power system. *Renew Energ* 99:379–389. <https://doi.org/10.1016/j.renene.2016.07.022>
- Deng HQ, Luo Y, Yao Y, Liu C (2013) Spring and summer precipitation changes from 1880 to 2011 and the future projections from CMIP5 models in the Yangtze River Basin, China. *Quatern Int* 304:95–106. <https://doi.org/10.1016/j.quaint.2013.03.036>
- Dibike Y, Prowse T, Shrestha R, Ahmed R (2012) Observed trends and future projections of precipitation and air temperature in the Lake Winnipeg watershed. *J Great Lakes Res* 38:72–82. <https://doi.org/10.1016/j.jglr.2011.04.005>
- Du Q, Kim AM, Zheng Y (2017) Modeling multimodal freight transportation scenarios in Northern Canada under climate change impacts. *Res Transport Bus Manag* 23:86–96
- Eum HI, Dibike Y, Prowse T (2017) Climate-induced alteration of hydrologic indicators in the Athabasca River Basin, Alberta,

- Canada. J Hydrol 544:327–342. <https://doi.org/10.1016/j.jhydr.2016.11.034>
- Fathalli B, Pohl B, Castel T, Safi MJ (2014) Evaluation of a surface temperature simulation over Tunisia using the WRF model. 3rd International Lund Regional-Scale Climate Modelling Workshop, 21st Century Challenges in Regional Climate Modelling, At Lund, Sweden
- Fu X, Kuo CC, Gan TY (2015) Change point analysis of precipitation indices of Western Canada. Int J Climatol 35:2592–2607. <https://doi.org/10.1002/joc.4144>
- Gaudard L, Romero F, Dalla Valle F, Gorret R, Maran S, Ravazzani G, Stoffel M, Volonterio M (2014) Climate change impacts on hydropower in the Swiss and Italian Alps. Sci Total Environ 493:1211–1221. <https://doi.org/10.1016/j.scitotenv.2013.10.012>
- Giorgi F, Jones C, Asrar GR (2009) Addressing climate information needs at the regional level: the CORDEX framework. World Meteorological Organization (WMO) Bulletin, 58(3):175
- Government of Canada (2019) Retrieved November 7, 2019 from <https://www.canada.ca/en/environment-climate-change/services/climate-change/canadian-centre-climate-services/basics/trends-projections/changes-temperature.html>
- Gutmann E, Pruitt T, Clark MP, Brekke L, Arnold JR, Raff DA, Rasmussen RM (2014) An intercomparison of statistical downscaling methods used for water resource assessments in the United States. Water Resour Res 50:7167–7186. <https://doi.org/10.1002/2014wr015559>
- Herrera-Pantoja M, Hiscock KM (2015) Projected impacts of climate change on water availability indicators in a semi-arid region of central Mexico. Environ Sci Policy 54:81–89. <https://doi.org/10.1016/j.envsci.2015.06.020>
- Hollander M, Wolfe DA (1973) Nonparametric statistical methods. John Wiley & Sons, New York, pp 68–75
- Hong SY, Noh Y, Dudhia J (2006) A new vertical diffusion package with an explicit treatment of entrainment processes. Mon Weather Rev 134:2318–2341. <https://doi.org/10.1175/Mwr3199.1>
- Houghton J (2007) Global warming, climate change and sustainability. John Ray Initiative Briefing Paper 14:2007
- Hutchinson MF, Mckenney DW, Lawrence K, Pedlar JH, Hopkinson RF, Milewska E, Papadopol P (2009) Development and testing of canada-wide interpolated spatial models of daily minimum-maximum temperature and precipitation for 1961–2003. J Appl Meteorol Clim 48:725–741. <https://doi.org/10.1175/2008j.amc1979.1>
- IPCC (2007) Climate change 2007: The physical science basis. Contribution of Working Group I to the Fourth Assessment Report of the Intergovernmental Panel on Climate Change. Cambridge University Press, Cambridge
- IPCC (Intergovernmental Panel on Climate Change). (2013). Climate change 2013: The physical science basis. Contribution of Working Group I to the Fifth Assessment Rep. of the Intergovernmental Panel on Climate Change, T. F. Stocker, et al. eds., Cambridge University Press, Cambridge, U.K., 1535
- Ishida K, Gorguner M, Ercan A, Trinh T, Kavvas ML (2017) Trend analysis of watershed-scale precipitation over Northern California by means of dynamically-downscaled CMIP5 future climate projections. Sci Total Environ 592:12–24
- Jha M, Pan ZT, Takle ES, Gu R (2004) Impacts of climate change on streamflow in the Upper Mississippi River Basin: a regional climate model perspective. J Geophys Res-Atmos. <https://doi.org/10.1029/2003jd003686>
- Jiang R, Gan TY, Xie J, Ni W, Kuo CC (2015) Historical and potential changes of precipitation and temperature of alberta subjected to climate change impact: 1900–2100. J Theor Appl Climatol. <https://doi.org/10.1007/s00704-015-1664-y>
- Kain JS (2004) The Kain–Fritsch convective parameterization: an update. J Appl Meteorol 43:170–181. [https://doi.org/10.1175/1520-0450\(2004\)043%3c0170:Tkcpau%3e2.0.Co;2](https://doi.org/10.1175/1520-0450(2004)043%3c0170:Tkcpau%3e2.0.Co;2)
- Karl TR, Nicholls N, Ghazi A (1999) CLIVAR/GCOS/WMO workshop on indices and indicators for climate extremes: workshop summary. Clim Change 42:3–7
- Kukal M, Irmak S (2016) Long-term patterns of air temperatures, daily temperature range, precipitation, grass-reference evapotranspiration and aridity index in the USA great plains: part II. Temporal trends. J Hydrol 542:978–1001. <https://doi.org/10.1016/j.jhydr.2016.06.008>
- Kuo CC, Gan TY (2018) Estimation of precipitation and air temperature over western Canada using a regional climate model. Int J Climatol 38:5125–5135. <https://doi.org/10.1002/joc.5716>
- Kuo CC, Gan TY, Higuchi K (2017) Evaluation of future streamflow patterns in lake simcoe subbasins based on ensembles of statistical downscaling. J Hydrol Eng. [https://doi.org/10.1061/\(ASCE\)He.1943-5584.0001548](https://doi.org/10.1061/(ASCE)He.1943-5584.0001548)
- Kurkute S, Li Z, Li Y, Huo F (2019) Assessment and projection of water budget over western canada using convection permitting WRF simulations. Hydrol Earth Syst Sci. <https://doi.org/10.5194/hess-2019-522>
- Lenderink G, Buishand A, van Deursen W (2007) Estimates of future discharges of the river Rhine using two scenario methodologies: direct versus delta approach. Hydrol Earth Syst Sc 11:1143–1159
- Lesack LFW, Marsh P, Hicks FE, Forbes DL (2014) Local spring warming drives earlier river-ice breakup in a large Arctic delta. Geophys Res Lett 41:1560–1566. <https://doi.org/10.1002/2013gl058761>
- Lim KSS, Hong SY (2010) Development of an effective double-moment cloud microphysics scheme with prognostic cloud condensation nuclei (CCN) for weather and climate models. Mon Weather Rev 138:1587–1612. <https://doi.org/10.1175/2009mwr2968.1>
- McKenney DW, Papadopol P, Campbell KL, Lawrence KM, Hutchinson MF (2006) Spatial models of Canada- and North America-wide 1971/2000 minimum and maximum temperature, total precipitation and derived bioclimatic variables. Marie: Canadian Forestry Service. Tech. note #: 106
- Mehrotra R, Sharma A (2010) Development and application of a multisite rainfall stochastic downscaling framework for climate change impact assessment. Water Resour Res. <https://doi.org/10.1029/2009wr008423>
- Mekis E, Vincent LA (2011) An overview of the 2<sup>nd</sup> generation adjusted daily precipitation dataset for trend analysis in Canada. Atmos Ocean 49:163–177. <https://doi.org/10.1080/0705900.2011.583910>
- Ozturk T, Turp MT, Turkes M, Kurnaz ML (2017) Projected changes in temperature and precipitation climatology of Central Asia CORDEX Region 8 by using RegCM4.3.5. Atmos Res 183:296–307. <https://doi.org/10.1016/j.atmosres.2016.09.008>
- Pacific Climate Impacts Consortium. (2014). “Statistically downscaled climate scenarios.” ([http://tools.pacificclimate.org/dataportal/downscaled\\_gcms/map/](http://tools.pacificclimate.org/dataportal/downscaled_gcms/map/)) (Jan 8, 2015)
- Pattnayak KC, Kar SC, Dalal M, Pattnayak RK (2017) Projections of annual rainfall and surface temperature from CMIP5 models over the BIMSTEC countries. Global Planet Change 152:152–166. <https://doi.org/10.1016/j.gloplacha.2017.03.005>
- Pendergrass AG, Hartmann DL (2014) Changes in the distribution of rain frequency and intensity in response to global warming. J Clim 27:8372–8383. <https://doi.org/10.1175/Jcli-D-14-00183.1>
- Perkins SE, Pitman AJ, Holbrook NJ, McAneney J (2007) Evaluation of the AR4 climate models' simulated daily maximum temperature, minimum temperature, and precipitation over Australia using

- probability density functions. *J Clim* 20:4356–4376. <https://doi.org/10.1175/Jcli4253.1>
- Peterson TC et al (2001) Report on the activities of the working group on climate change detection and related rapporteurs 1998–2001. WMO, Rep. WCDMP-47, WMO-TD 1071, Geneve, Switzerland
- Riahi K, Rao S, Krey V, Cho CH, Chirkov V, Fischer G, Kindermann G, Nakicenovic N, Rafaj P (2011) RCP 8.5-A scenario of comparatively high greenhouse gas emissions. *Clim Change* 109:33–57. <https://doi.org/10.1007/s10584-011-0149-y>
- Scheepers H, Wang J, Gan TY, Kuo CC (2018) The impact of climate change on inland waterway transport: effects of low water levels on the Mackenzie River. *J Hydrol* 566:285–298. <https://doi.org/10.1016/j.jhydrol.2018.08.059>
- Sen PK (1968) Estimates of the regression coefficient based on Kendall's tau. *J Am Stat Assoc* 63(324):1379–1389
- Shashikanth K, Madhusoodhanan CG, Ghosh S, Eldho TI, Rajendran K, Murtugudde R (2014) Comparing statistically down-scaled simulations of Indian monsoon at different spatial resolutions. *J Hydrol* 519:3163–3177. <https://doi.org/10.1016/j.jhydr.2014.10.042>
- Skamarock WC, Klemp JB, Dudhia J, Gill DO, Barker DM, Duda M, Huang XY, Wang W, Powers JG (2008) A description of the advanced research WRF version 3. NCAR tech. note, NCAR/TN\ u2013475?STR, 123 pp
- Stewart RE, Leighton HG, Marsh P, Moore GWK, Ritchie H, Rouse WR, Soulis ED, Strong GS, Crawford RW, Kochtubajda B (1998) The Mackenzie GEWEX Study: the water and energy cycles of a major North American river basin. *Bull Am Meteorol Soc* 79(12):2665–2684
- Tan X, Gan TY (2015) Contribution of human and climate change impacts to changes in streamflow of Canada. *Sci Rep* 5:17767. <https://doi.org/10.1038/srep17767>
- Tan ML, Ibrahim A, Yusop Z, Chua VP, Chan NW (2017) Climate change impacts under CMIP5 RCP scenarios on water resources of the Kelantan River Basin, Malaysia. *Atmos Res* 189:1–10. <https://doi.org/10.1016/j.atmosres.2017.01.008>
- Trang NTT, Shrestha S, Shrestha M, Datta A, Kawasaki A (2017) Evaluating the impacts of climate and land-use change on the hydrology and nutrient yield in a transboundary river basin: a case study in the 3S River Basin (Sekong, Sesan, and Srepok). *Sci Total Environ* 576:586–598. <https://doi.org/10.1016/j.scitotenv.2016.10.138>
- Vincent LA, Wang XLL, Milewska EJ, Wan H, Yang F, Swail V (2012) A second generation of homogenized Canadian monthly surface air temperature for climate trend analysis. *J Geophys Res-Atmos.* <https://doi.org/10.1029/2012jd017859>
- Watson DF (1992) Contouring: a guide to the analysis and display of spatial data. Pergamon Press, Oxford, England
- Watson DF, Philip GM (1984) Triangle based interpolation. *Math Geol* 16(8):779–795. <https://doi.org/10.1007/BF01036704>
- Whitehead PG, Crossman J, Balana BB, Futter MN, Comber S, Jin L, Skuras D, Wade AJ, Bowes MJ, Read DS (2013) A cost-effectiveness analysis of water security and water quality: impacts of climate and land-use change on the River Thames system. *Philos T R Soc A.* <https://doi.org/10.1098/rsta.2012.0413>
- Wilson CO, Weng QH (2011) Simulating the impacts of future land use and climate changes on surface water quality in the Des Plaines River watershed, Chicago Metropolitan Statistical Area, Illinois. *Sci Total Environ* 409:4387–4405. <https://doi.org/10.1016/j.scitotenv.2011.07.001>
- Woo MK, Thorne R (2003) Streamflow in the Mackenzie basin, Canada. *Arctic* 328–340
- Woo MK, Thorne R, Giguère N (2014) Winter flows in the Mackenzie drainage system. *Arctic* 67(2):238–256
- Xia XH, Wu Q, Mou XL, Lai YJ (2015) Potential impacts of climate change on the water quality of different water bodies. *J Environ Inform* 25:85–98. <https://doi.org/10.3808/jei.201400263>
- Yang DQ, Shi XG, Marsh P (2015) Variability and extreme of Mackenzie River daily discharge during 1973–2011. *Quatern Int* 380:159–168. <https://doi.org/10.1016/j.quaint.2014.09.023>
- Zhang X, Flato G, Kirchmeier-Young M, Vincent L, Wa H, Wang C, Rong R, Fyfe J, Li G, Kharin VV (2019) Changes in temperatures and precipitation across Canada: chapter 4. In: Bush E, Lemmen DS (eds) Canada's changing climate report. Government of Canada, Ottawa, pp 112–193
- Zheng YZ, Kim AM (2017) Rethinking business-as-usual: Mackenzie River freight transport in the context of climate change impacts in northern Canada. *Transport Res D-Tr E* 53:276–289. <https://doi.org/10.1016/j.trd.2017.04.023>

**Publisher's Note** Springer Nature remains neutral with regard to jurisdictional claims in published maps and institutional affiliations.